Adv Physiol Educ 28: 160–179, 2004;
doi:10.1152/advan.00045.2004.

REFRESHER COURSE | *Cellular Homeostasis*

Regulation of intracellular pH

Walter F. Boron

Department of Cellular and Molecular Physiology, Yale University School of Medicine, New Haven, Connecticut 06520-8026

Received 13 September 2004; accepted in final form 17 September 2004

Boron, Walter F. Regulation of intracellular pH. *Adv Physiol Educ* 28: 160–179, 2004; doi:10.1152/advan.00045.2004.—The approach that most animal cells employ to regulate intracellular pH (pH_i) is not too different conceptually from the way a sophisticated system might regulate the temperature of a house. Just as the heat capacity (C) of a house minimizes sudden temperature (T) shifts caused by acute cold and heat loads, the buffering power (β) of a cell minimizes sudden pH_i shifts caused by acute acid and alkali loads. However, increasing C (or β) only minimizes T (or pH_i) changes; it does not eliminate the changes, return T (or pH_i) to normal, or shift steady-state T (or pH_i). Whereas a house may have a furnace to raise T, a cell generally has more than one acid-extruding transporter (which exports acid and/or imports alkali) to raise pH_i. Whereas an air conditioner lowers T, a cell generally has more than one acid-loading transporter to lower pH_i. Just as a house might respond to graded decreases (or increases) in T by producing graded increases in heat (or cold) output, cells respond to graded decreases (or increases) in pH_i with graded increases (or decreases) in acid-extrusion (or acid-loading) rate. Steady-state T (or pH_i) can change only in response to a change in chronic cold (or acid) loading or chronic heat (or alkali) loading as produced, for example, by a change in environmental T (or pH) or a change in the kinetics of the furnace (or acid extrudes) or air conditioner (or acid loaders). Finally, just as a temperature-control system might benefit from environmental sensors that provide clues about cold and heat loading, at least some cells seem to have extracellular CO_2 or extracellular HCO_3^- sensors that modulate acid-base transport.

hydrogen ions; bicarbonate; exchanger; cotransporter

INTRACELLULAR pH (pH_i), which for our purposes we will regard as the pH of the aqueous cytosolic solution, is a parameter that is of interest to most biologists. The reason for this interest is that changes in pH_i affect the ionization state of all weak acids and weak bases–a bewildering array of cellular molecules that includes all peptides and proteins–and thus may potentially affect a wide array of biological processes. Not surprisingly, all animal cells that have been examined, aside from non-nucleated erythrocytes, vigorously regulate their pH_i (36). They do this by sensing changes in pH_i and then appropriately speeding up or slowing down various transporters that move acids and/or bases across the plasma membrane.

Many nonspecialists find it difficult to think about pH_i and pH_i regulation. After all, the pH scale is upside down (increases in pH_i correspond to decreases in $[H^+]$), and protons have the disconcerting habit of binding to molecules (at any time, more than 99.99% of available protons are bound to "buffers"). Moreover, if a proton dissociates from a buffer and collides with a water molecule, this proton may become part of a perfectly respectable H_2O molecule, but simultaneously cause a completely different proton to pop off from another H_2O molecule some distance away—an example of the effects of a proton wire.

Sound complicated? It is and it isn't. "It is" in the sense that any biological process is complex when one considers it at the molecular level. However, my PhD mentor, the venerable Albert Roos, now retired from Washington University School of Medicine and approaching his 90th birthday, used to tell me that if a scientist really understands his or her work, the scientist should be able to explain the essence of that work to the average person on the street. Thus my job in this review should be rather easy: I must only explain pH_i regulation to the physiologist on the street.

As it happens, the way cells approach the problem of pH_i regulation is not so different–conceptually, at least–from the way we might approach the problem of regulating the temperature in a house. Just as a furnace makes the temperature go up, transporters called "acid extruders" (which move H^+ out of the cell and/or move bases such as HCO_3^- into the cell) make pH_i go up. Similarly, just as an air conditioner makes the temperature go down, transporters called "acid loaders" (which move H^+ into the cell and/or move bases such as HCO_3^- out of the cell) make pH_i go down. In this review, we will develop a model of temperature regulation that we will subsequently apply to pH_i regulation. Every hypothetical example of a rise or fall in temperature corresponds to an analogous real-life instance of a rise or fall in pH_i.

Address for reprint requests and other correspondence: W. F. Boron, Dept. of Cellular and Molecular Physiology, Yale Univ. School of Medicine, 333 Cedar St., New Haven, CT 06520 (E-mail: walter.boron@yale.edu).

The reader is directed to a website (http://www.the-aps.org/education/refresher/CellRefresherCourse.htm) that includes the PowerPoint slideshow that I presented during my oral presentation at Experimental Biology 2004, on April 17, 2004.

Temperature Regulation in a House

Heat capacity. Imagine that our house has an initial temperature (T) of 22°C. Imagine also that our house has a heat capacity (C) of 50×10^6 cal/°C. This value is equivalent to that of 50,000 kg of H_2O (a 50-m^3 pool of water).

We will now suddenly inject into our house 50×10^6 calories of heat; this is roughly the amount that would be given off by a 1,000-W electrical heater over a period of 2.4 days. If we wait long enough for the injected heat to equilibrate with the mass of the house—and if no other processes add or withdraw heat—the temperature will increase by precisely 1°C:

$$\Delta T = \frac{50 \times 10^6 \text{ cal}}{50 \times 10^6 \text{ cal/°C}} = 1\text{°C} \qquad (1)$$

In other words, the temperature of our house will rise from 22°C to 23°C.

If we introduce a 50-m^3 indoor swimming pool into our house, the heat capacity will double to 100×10^6 cal/°C. Thus a heat load of 50×10^6 calories will cause the temperature to increase by only 0.5°C

$$\Delta T = \frac{50 \times 10^6 \text{ cal}}{100 \times 10^6 \text{ cal/°C}} = 0.5\text{°C} \qquad (2)$$

Because the magnitude of the temperature change is inversely proportional to the heat capacity, raising the heat capacity of the house increases the ability to resist temperature fluctuations. In other words, heat capacity represents the ability to "buffer" loads of heat or cold, just as buffering power (β) in a cell represents the ability to resist pH_i fluctuations in the face of loads of alkali or acid. However, raising the heat capacity (or β) does not eliminate temperature (or pH_i) fluctuations, it only reduces their magnitude. Moreover, once we have imposed a heat/cold load (or alkali/acid load) and observed the resulting increase/decrease in temperature (or pH_i), subsequently raising the heat capacity (or β) does not return the temperature (or pH_i) to its initial value, which would be 22°C in our temperature example.

The last statement in the previous paragraph is worthy of some clarification. Consider our example in *Eq. 1*, in which C is 50×10^6 cal/°C. Imposing a heat load of 50×10^6 calories will cause the temperature to rise from 22 to 23°C. If we now double the heat capacity by adding 50,000 kg of water with a temperature of 23°C, the temperature of the house (and that of the water that we just added) will remain at 23°C. If we had instead added 50,000 kg of water with a temperature of 22°C, the temperature of the house would fall by 0.5°C, and that of the water would rise by the same amount. However, this maneuver of adding 22°C water to the 23°C house simultaneously did two things: *1*) it raised the heat capacity and *2*) it injected a "cold" load. In analyzing the effects of various maneuvers—both in our temperature-regulation model and in pH_i regulation—we must constantly be vigilant to identify such dual effects.

Perturbations: Acute and Chronic Heat/Cold Loads

Acute heat loads. In a house, appliances can impose a heat load: hot plates, toasters, ovens, clothes dryers, irons, and water heaters, to name a few. On a hot day, opening an exterior door imposes a heat load on an air-conditioned house. These heat loads I will define as "acute," acute as opposed to "chronic," which we will discuss later. The most critical attributes of acute heat loads is that they exert their effects over a *limited period of time* that is—from the perspective of our observations—*relatively brief*. Thus we can easily describe the absolute magnitude of the heat load. For example, if one turns on a 1,000-W hair drier for 2 min, the imposed heat load is

$$\text{Heat load} = (1{,}000 \text{ W}) \times \frac{\text{joule/s}}{1 \text{ W}} \times \frac{1 \text{ calorie}}{4.2 \text{ joules}} \times (120 \text{ s}) = 28.6 \times 10^3 \text{ calories} \qquad (3)$$

Moreover, we can predict that this acute heat load will raise the temperature of our house (the one without the swimming pool) by 0.000, 57°C:

$$\Delta T = \frac{28.6 \times 10^3 \text{ calories}}{50 \times 10^6 \text{ cal/°C}} = 0.000\,57\text{°C} \qquad (4)$$

Later, we will see that acutely loading a cell with a known amount of alkali will produce a pH_i increase, the magnitude of which we can predict-using an equation analogous to Equation 4-if we know the buffering power.

Chronic heat loads. Unlike the heat sources discussed above, those that impose a chronic heat load exert their effects over an *indefinite period of time* that—from the perspective of our observations—is *relatively long*. For example, on a sunny summer day, the heat introduced from the environment by radiation, conduction, and convection may impose a heat load for many hours. Chronic heat loaders are best described in terms of the *rate* at which they impose a heat load, inasmuch as it is impossible to predict the total heat load.

In our temperature-regulation model, the distinction between acute and chronic heat loads is somewhat artificial. For example, if we inadvertently left an iron "on" indefinitely, the iron would become a *chronic* heat loader. In moderate climates, the heat load imposed by sun has a predictably limited duration (i.e., daylight hours); does the sun then become an *acute* heat loader? Nevertheless, when we turn to pH_i regulation, we will see that alkali loads to a cell usually segregate rather neatly into those with either a limited duration (and thus magnitude), such as exposing a cell to a permeant weak base, or an indefinite duration (and thus magnitude), such as stimulating a transporter that continually imports HCO_3^- into the cell.

Acute cold loads. Our house might also have a few mechanisms for imposing acute cold loads, such as frozen food left to thaw on the kitchen counter, or a refrigerator with an open door. On a cold winter day, we could impose a more substantial acute cold load by temporarily opening an exterior door. Each of these mechanisms exerts its effects over a *limited and relatively short period of time*, and thus withdraws a limited amount of energy from our house. The counterpart in pH_i regulation might be the acute acid load imposed by exposing a cell to a permeant weak acid.

Chronic cold loads. During the winter, the heat loss from our house to the environment represents a chronic cold load. By

analogy to chronic heat loaders, chronic cold loaders are best described in terms of the *rate* at which they impose a cold load. The counterpart in pH_i regulation might be the chronic acid load imposed by a transporter that continually imports H^+ or exports HCO_3^-.

Regulation: Furnaces and Air Conditioners

A "dumb" temperature-control system. Having mastered the concepts of heat capacity and the various kinds of heat and cold loads, we are in a position to discuss temperature regulation. Like any physiological regulatory system, our temperature-regulating system must have certain key components:

- A temperature sensor,
- A coordinating center, and
- Effectors for injecting heat into and/or withdrawing heat from our house.

In our first example (Fig. 1*A*), the system will work like that in a typical house. The furnace will have two speeds ("off" and "on"), and the coordinating center will turn on the furnace whenever the temperature falls below 20°C. The air conditioner also will have two speeds ("off" and "on"), and the coordinating center will turn on the air conditioner whenever the temperature rises above 24°C. If the furnace and air conditioner are sufficiently powerful, the temperature-control system will insure that the temperature does not fall far below 20°C, nor does not rise far above 24°C.

A "smart" temperature-control system. Although the above temperature-control system would be fine for most purposes, the temperature would tend to oscillate, which might be unsatisfactory if our house contained an instrument with a very high temperature sensitivity. The more sophisticated temperature-control system outlined in Fig. 1*B* would be more effective at stabilizing the temperature in the face of acute heat and cold loads. In this example, the furnace would be "on" at virtually all times. However, its heat output would increase linearly as temperature fell. Similarly, the air conditioner would be "on" virtually continuously, but its rate of heat withdrawal would increase linearly as the temperature rose. Thus the furnace really is a specialized (i.e., regulated) chronic heat loader, and the air conditioner is a specialized (i.e., regulated) chronic cold loader. If the furnace were the *only* chronic heat loader, and if the air conditioner were the *only* cold loader, then the steady-state temperature would be defined by the intersection of the curves describing the temperature dependencies of the furnace and air conditioner. Although the arrangement depicted in Fig. 1*B* would produce a far more stable temperature than in our first example, this level of control would come at a high price—low energy efficiency—because the furnace and air conditioner would continuously fight each other.

Later, we will see that cells use acid-extruding transporters (analogous to furnaces) that raise pH_i, more so as pH_i falls. Moreover, cells have acid-loading transporters (analogous to air conditioners) that lower pH_i, more so as pH_i rises. In the steady state, these two sets of transporters continuously fight each other, consuming metabolic energy-the price that life is willing to pay for the sake of control.

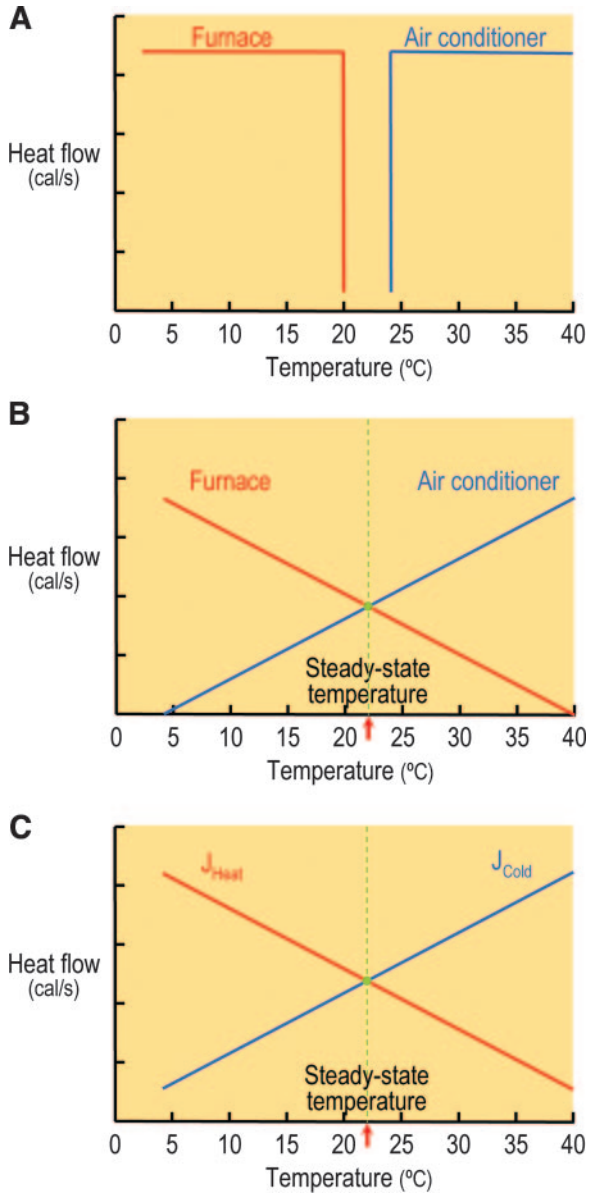

Fig. 1. The temperature (T) dependencies of hypothetical furnaces and air conditioners. *A*: "dumb" temperature controller. Here, the furnace produces heat at a fixed rate whenever the temperature falls below a threshold of 20°C. Similarly, the air conditioner withdraws heat at a fixed rate whenever the temperature rises above a threshold of 24°C, which must be above the threshold for the furnace. *B*: "smart" temperature controller. Here, the furnace is always on, but its rate of heat production increases linearly as the temperature falls. Conversely, the rate at which the air conditioner withdraws heat increases linearly as the temperature rises. If the furnace is the only chronic heat loader, and if the air conditioner is the only chronic cold loader, then the system is in a steady state at 22°C, when the rates of heat loading (J_{heat}) and cold loading (J_{cold}) are equal. *C*: "smart" temperature controller with lumped J_{heat}-vs.-T and J_{cold}-vs.-T parameters. Here, we combine the temperature dependence of the furnace with that of all nonregulatory chronic heat loaders to obtain J_{heat}. Similarly, we combine the temperature dependence of the air conditioner with that of all non-regulatory chronic cold loaders to obtain J_{cold}. cal, calorie.

Total heat and cold loading. Another way of approaching the analysis of the sophisticated temperature-control system would be to lump the heat output of the furnace with that of all other chronic heat loaders that are not part of our temperature-control system. The result is the *total chronic heat loading*

(J_{heat}). Similarly, we also could lump the heat withdrawal of the air conditioner with that of all other chronic cold loaders, arriving at the *total chronic cold loading* (J_{cold}). If these "other," non-regulatory chronic heat and cold loaders have relatively low temperature dependencies, then the temperature dependency of J_{heat} and J_{cold} in Fig. 1*C* would have shapes similar to the "Furnace" and "Air conditioner" curves in Fig. 1*B*. However, at any temperature, the curves would have higher values in Fig. 1*C*. Nevertheless, the steady-state temperature would still be described by the intersection of the two curves.

Later, we will see that the total chronic acid extrusion in cells reflects transporters that extrude acid (analogous to furnaces) and—under special circumstances—passive chronic alkali loading (analogous to nonregulatory chronic heat loading). Similarly, the total chronic acid loading in cells reflects transporters that load the cell with acid (analogous to air conditioners) as well as passive acid loading (analogous to nonregulatory chronic cold loading).

We should *not* regard the curves in Fig. 1*C* as immutable. For example, during the winter, the nonregulatory component of J_{cold} (or chronic acid loading for a cell) would be higher at night (or when extracellular pH is low) than during the warmer daytime hours (or when extracellular pH is high). Moreover, the slope of the J_{cold}-vs.-T relationship (or the acid loading vs. pH_i relationship) would decrease if the air conditioner's filter became clogged (or if the cell down-regulated an acid loader). On the other hand, the slope would increase if a fall in outside temperature made the air conditioner more efficient (or if a change in ion gradients made an acid loader more efficient). The J_{heat}-vs.-T relationship would be subject to comparable changes. In other words, the curves in Fig. 1*C* describe the temperature dependencies of chronic heat and cold loading under a defined set of conditions that are subject to alteration.

Response to an acute cold load. Our sophisticated temperature-control system is now ready for a challenge. Imagine that it is a frigid winter's evening, and that the temperature of our house is at a stable 22°C. Under these starting conditions, J_{heat} exactly matches J_{cold}, as represented by the intersection of the two curves in Fig. 2*A*. A blast of cold air through a temporarily open door now lowers the temperature from 22°C to 4°C (*step 1* in Fig. 2*A*). Sensing this decrease in temperature, our control system increases the heat output of the furnace and simultaneously lowers the cold output of the air conditioner (*step 2* in Fig. 2*A*). Similarly, cells will respond to a sudden decrease in pH_i by stimulating their acid extruders and inhibiting acid loaders. Returning to our temperature-regulation model, because J_{heat} is now far greater than J_{cold}, the temperature begins to rise. How fast? Consider a more general representation of *Eq. 1*:

$$\underbrace{\Delta T}_{°C} = \frac{\overbrace{\text{Heat Added} - \text{Cold Added}}^{\text{Cal}}}{\underbrace{\text{Heat Capacity}}_{\text{cal/°C}}} \qquad (5)$$

The numerator of the above equation is simply the net amount of heat added. Thus a net addition of heat raises the temperature (a positive number), a net withdrawal of heat (a negative-number) lowers the temperature. Of course, the temperature is stable when the net addition of heat is nil.

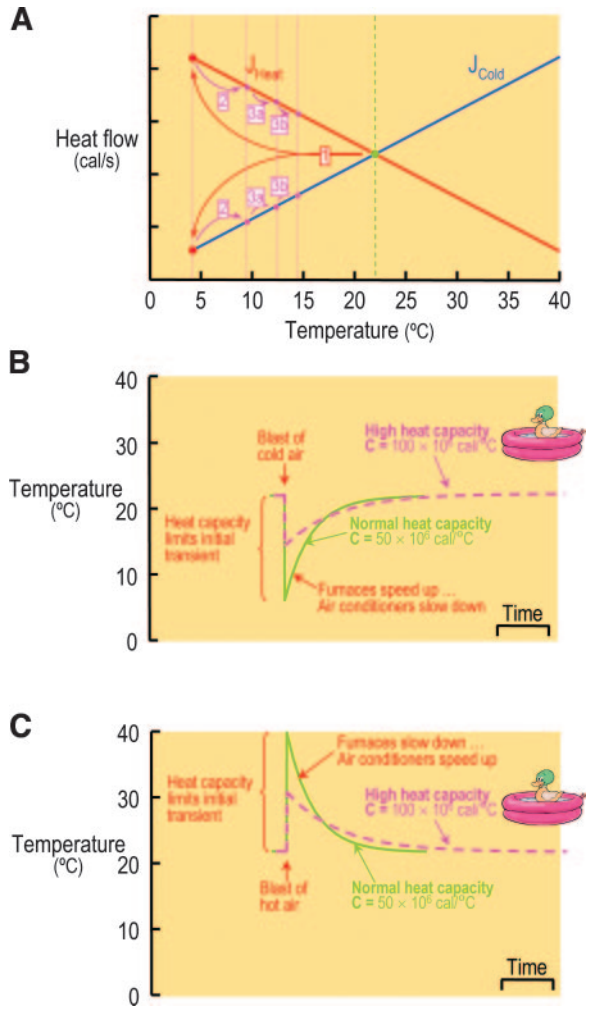

Fig. 2. Response to acute cold and heat loads. *A*: effect of an acute cold load on J_{heat} and J_{cold}. After the sudden decrease in temperature (*step 1*), temperature at first increases rapidly (*step 2*) because J_{heat} greatly exceeds J_{cold}. As temperature gradually recovers, the rate of temperature increase slows (*steps 3a and 3b*) until the temperature eventually reaches its initial value at the intersection of the red and blue curves. *B*: time course of temperature in response to an acute cold load. At any instant in time, the rate of the temperature recovery is proportional to the difference ($J_{heat} - J_{cold}$), but inversely proportional to heat capacity. *C*: time course of temperature in response to an acute heat load. In this example, the blast of hot air introduces as much heat as was removed by the blast of cold air in the example in panels *A* and *B*.

We now transform this equation by dividing both sides by the time interval Δt:

$$\frac{\Delta T}{\Delta t} = \frac{(\text{Heat Added})/\Delta t - (\text{Cold Added})/\Delta t}{\text{Heat Capacity}} \qquad (6)$$

$$\frac{\Delta T}{\Delta t} = \frac{J_{heat} - J_{cold}}{C}$$

In other words, the rate of temperature increase is proportional to the difference between the chronic rates of heat loading and cold loading, and the proportionality constant is the reciprocal of heat capacity. Thus, if the heat capacity were

infinite, the temperature would never change, whereas if the heat capacity were very low, even small differences between J_{heat} and J_{cold} would lead to rapid temperature changes. We might regard *Eq. 6* as the fundamental law of temperature regulation. As we will see in *Eqs. 21* and *22*, a comparable law exists for pH_i regulation in cells.

Returning now to *step 2* in Fig. 2*A*, we can appreciate that the difference $J_{heat} - J_{cold}$, and thus the rate at which the temperature increases, is maximal immediately after the blast of cold air–when the temperature is lowest. As temperature increases, the rate of heat production by the furnace gradually decreases and the rate of heat withdrawal by the air conditioner gradually increases. Thus, the difference ($J_{heat} - J_{cold}$) gradually becomes smaller until, at the original temperature of 22°C, $J_{heat} = J_{cold}$ and the system returns once again to its original steady state (i.e., $\Delta T/\Delta t = 0$). Similarly for cells that are recovering from an acute acid load, the difference between acid-loading and acid-extrusion rates is greatest when pH_i is lowest, and gradually falls to zero as pH_i rises toward its original steady-state value. During the course of a temperature recovery, the net amount of heat introduced by the temperature-control system (i.e., the increment in $J_{heat} - J_{cold}$ integrated over time) is exactly equal to the net amount of cold introduced by the blast of cold air. We can make a comparable statement for cells, where the net amount of alkali extruded during a pH_i recovery exactly equals the amount of acid introduced by the insult—acute acid load.

The solid curve in Fig. 2*B* illustrates the hypothetical time course of the temperature recovery when the house has a normal heat capacity. If we wished to be more precise, we could express *Eq. 6* as a differential equation, which we could solve to obtain an exponential expression that would describe the time course of T vs. time (*t*). Knowing the heat capacity of our house and the amount of heat withdrawn by the blast of cold air, we could compute the initial ΔT. Knowing the actual value of J_{heat} and J_{cold} over the relevant range of temperatures, we could compute the entire time course of T vs. *t* from the instant of the big blast to the eventual reachievement of the steady state.

The dashed curve in Fig. 2*B* illustrates how the system would respond if we were to double the heat capacity of our house (or buffering power of a cell) by adding that 50-m^3 swimming pool (or buffers to a cell). Notice that, for the same acute cold load (or acute acid load), the magnitude of the initial temperature (or pH_i) decrease is half of what it was before. Also notice that the time course of the exponential recovery of temperature (or pH_i) is stretched out by a factor of 2 (i.e., the time constant has doubled). Nevertheless, the total amount of heat withdrawn by the blast of cold air (or acid introduced by the acute acid load) equals the net amount of heat (or alkali) subsequently introduced by the temperature-control (or pH_i control) system, and both values are identical to their counterparts in the first example (solid curve in Fig. 2*B*), in which the heat capacity (or β) was normal.

Response to an acute heat load. The solid curve in Fig. 2*C* illustrates the hypothetical response of our temperature-control (or pH_i control) system, assuming a normal heat capacity (or β), to an acute heat (or alkali) load, such as we might observe upon opening an exterior door on a hot summer day (or injecting a cell with alkali). For the sake of symmetry, we assume that the magnitude of the acute heat load in this example is exactly the same as the magnitude of the acute cold in the previous one. Thus the blast of hot air causes the temperature to rise to 40°C. Our temperature-control (or pH_i control) system will respond by immediately reducing the rate of heat output by the furnace (or acid extrusion) and increasing the rate of heat withdrawal by the air conditioner (or acid loading), in a manner analogous to that shown in Fig. 2*A*. As a result, the temperature (or pH_i) falls with an exponential time course, with J_{heat} (or the chronic acid-extrusion rate) gradually rising and J_{cold} (or the chronic acid loading rate) gradually falling until these two parameters once again come into balance at the original temperature of 22°C (or pH_i).

As we saw in the blast-of-cold-air example, doubling the heat capacity reduces the initial ΔT by a factor of 2 and increases the time constant of the temperature recovery by a factor of 2. However, the final temperature is the same.

It is worth emphasizing three points. First, a high heat capacity (or buffering power) can reduce the magnitude of a temperature (or pH_i) perturbation, but cannot eliminate the perturbation. Second, the magnitude of the heat capacity (or buffering power) has no effect whatsoever on the final steady-state temperature (or pH_i). Third, final steady-state temperature (or pH_i) depends solely on the relationship between J_{heat} (chronic acid extrusion) and J_{cold} (chronic acid loading).

Regarding this last point, as long as both J_{heat}-vs.-T and J_{cold}-vs.-T remain unchanged, the final steady-state temperature must also remain unchanged. As we will see in the next section, the steady-state temperature can change only as the result of a fundamental change in the kinetics of J_{heat} and/or J_{cold}.

The recovery of temperature in Fig. 2, *B* and *C*, is an indication of *temperature regulation*, the ability of the system-complete with its system of sensors, a coordinating center, and effectors-to return temperature to some steady-state value. To quantify temperature regulation, we focus on the *rate* at which the system can return temperature to normal following an acute cold or heat load. We might express this rate as an absolute rate of temperature recovery (d*T*/d*t*, expressed as°C/s) measured at some defined temperature, a series of d*T*/d*t* values measured over a range of temperatures, or as the time constant (measured in seconds) that characterizes the trajectory of the temperature recovery. We will see later that we can use analogous terms to quantitate pH_i regulation.

Changes in steady-state temperature. As we noted in our discussion of Fig. 1*C*, the J_{heat} and J_{cold} curves could change due to alterations in nonregulatory heat or cold loading, or to changes in the furnace and air conditioner themselves. In this section, we will examine three examples that illustrate how changes in J_{heat} and/or J_{cold} affect steady-state temperature as well as the time course of temperature as the system achieves a new steady state.

Response to inhibiting the furnace. We begin our first experiment in this series with normal J_{heat}-vs.-T and J_{cold}-vs.-T profiles, and thus a normal steady-state temperature of 22°C. What would happen if—in an instant—we were to reduce the output of our furnace by a constant fraction across a wide range of temperatures? In Fig. 3*A*, we represent such a fall in heat flow by decreasing the negative slope of the J_{heat}-vs.-T curve (dashed red curve in Fig. 3*A* and *step 1* in Fig. 3*A*). At the instant of the perturbation, the temperature would still be 22°C. However, because we have rotated the J_{heat}-vs.-T curve down-

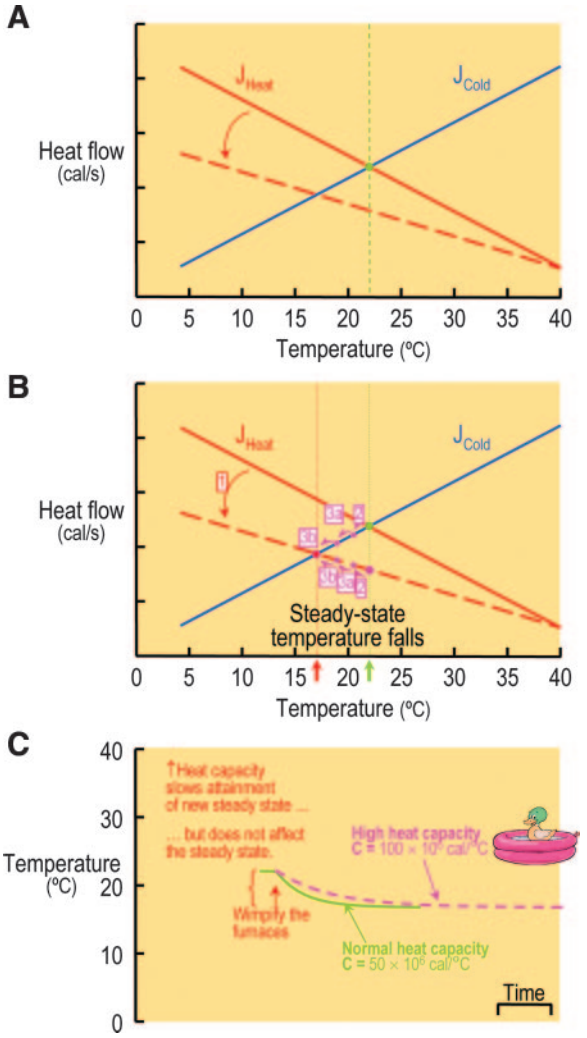

Fig. 3. Response to a sudden decrease in the rate of heat production. *A*: dependence of J_{heat} and J_{cold} on temperature. Inhibition of the furnace is represented by a decrease in the slope of the J_{heat}-vs.-temperature relationship (dashed line). *B*: changes in J_{heat} and J_{cold} as temperature falls. Immediately after the decrease in J_{heat} (*step 1*), J_{cold} exceeds J_{heat} by a modest amount. Thus temperature initially falls at a moderate rate (*step 2*). As temperature continues to fall, the difference between J_{cold} and J_{heat} decreases (*steps 3a* and *3b*), until the two values eventually come into balance at a temperature of 17°C. *C*: time course of temperature. At any instant in time, the rate of the temperature decline is proportional to the difference ($J_{cold} - J_{heat}$), but inversely proportional to heat capacity.

ward, J_{heat} at 22°C is now substantially less than J_{cold} at 22°C. As a result, $J_{heat} - J_{cold}$ is a relatively large negative number, so that according to *Eq. 6*, temperature begins to fall rather rapidly (*step 2* in Fig. 3*B*). As the temperature falls, however, J_{heat} gradually rises and J_{cold} gradually falls until the two come into balance at a new, lower, steady-state temperature that, in this example, is 17°C (*step 3a* and *3b* in Fig. 3*A*). The solid curve in Fig. 3*C* shows the time course of temperature for a normal heat capacity.

Later, in Fig. 15*A*, we will see that inhibiting acid extrusion, in the face of continuing acid loading, causes steady-state pH_i to fall in a manner analogous to that outlined for temperature in Fig. 3.

If we double the heat capacity of the house by adding our 50-m^3 swimming pool (dashed curve in Fig. 3*C*), the temperature falls only half as rapidly as before, but the final temperature is the same 17°C. Thus raising the heat capacity (of buffering power) slows the attainment of the steady state, but has no effect on the steady-state temperature (or pH_i), or on the rates of heat production (or acid extrusion) or withdrawal (or acid loading) in the new steady state.

Response to stimulating nonregulatory cooling. Rather than inhibiting the furnace (or an acid extruder), as in the previous example, we can produce an identical decrease in steady-state temperature (or pH_i) either by stimulating the air conditioner (or an acid loader) or by lowering the outside temperature (or extracellular pH). In this next temperature-regulation example, we will do the latter by raising the non-regulatory component of J_{cold} by a constant fraction across a wide range of temperatures. We represent this effect in Fig. 4*A* the increased cooling by increasing the slope of the J_{cold}-vs.-T curve (dashed curve). At the instant of the perturbation, J_{cold} is now substantially greater than J_{heat} at 22°C. As in the previous example, $J_{heat} - J_{cold}$ is now a relatively large negative number, so that temperature begins to fall rather rapidly. Eventually, the falling temperature brings J_{heat} and J_{cold} into balance at the same new, lower, steady-state temperature as in the previous example. The solid and dashed curves in Fig. 4*B* are exactly the same curves that described the time course of temperature when we inhibited the furnace in Fig. 3*B*.

An important lesson from the two hypothetical experiments in Figs. 3 and 4 is that monitoring temperature (or pH_i) as it approaches a new steady state tells us little about the underlying cause(s) of the shift in steady-state temperature (or pH_i). If

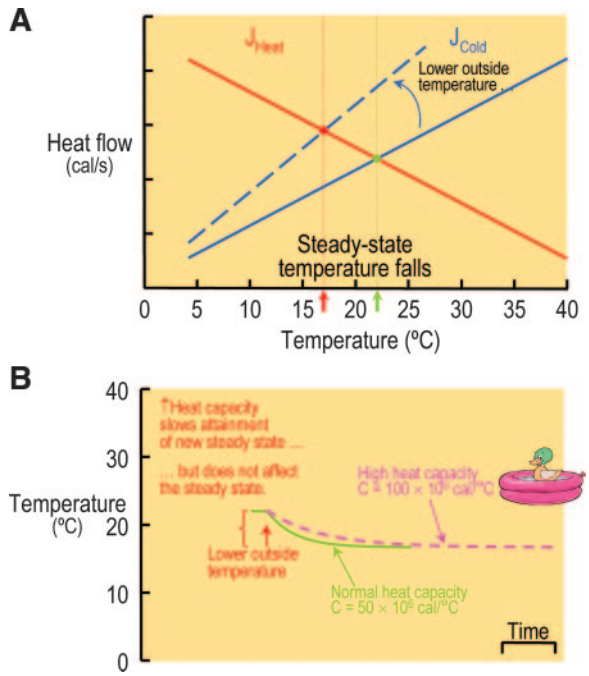

Fig. 4. Response to a sudden increase in the rate of heat withdrawal. *A*: dependence of J_{heat} and J_{cold} on temperature. The increase in nonregulatory chronic cold loading is represented by an increase in the slope of the J_{cold}-vs.-temperature relationship (dashed line). *B*: time course of temperature. Note that the final temperature in this example (17°C) is the same as in Fig. 3, although the thermal insults were quite different. Thus, neither the change in steady-state temperature, nor even the time course of the temperature change, provide specific information about the underlying mechanism of the thermal insult.

the steady-state temperature (or pH_i) falls, for example, we cannot conclude that J_{heat} (or the chronic acid-extrusion rate) has been reduced or that J_{cold} (or the chronic acid-loading rate) has been augmented. Neither can we come to conclusions about the disposition of the furnace (or acid-extruding transporters) vs. nonregulatory mechanisms of heat loading (or passive alkali-loading mechanisms), or about the disposition of the air conditioner (or acid-loading transporters) vs. nonregulatory mechanisms of cold loading (or passive alkali-loading mechanisms). All that we can conclude is the following: some change has occurred that–as monitored at the previous steady-state temperature (or pH_i)–has caused J_{cold} (or the chronic acid-loading rate) to become greater than J_{heat} (or the chronic acid-extrusion rate). This inequality (i.e., $J_{cold} > J_{heat}$) could have come about in many different ways . . . but in each case, the temperature (or pH_i) begins to fall . . . and the temperature (or pH_i) will continue to fall until J_{heat} (or chronic acid-loading rate) and J_{cold} (or chronic acid-extrusion rate) once again come into balance. If we wish to learn more about the mechanism of the insult that led to a decrease in steady-state temperature (or temperature), we could repeat the experiment under conditions in which we have specifically blocked (or stimulated) particular components of the control system. Alternatively, we could repeat the experiment on a duplicate house that lacks a furnace (or on a cell with a knocked-out acid extruder), or that has a furnace with a known functional change (or a cell with a mutated acid extruder).

Response to compound perturbations. Imagine that it is a gorgeous late summer's day with an outside temperature of 28°C. All the windows of the house are open. While you are on a walk, a cold front moves in and lowers the outside temperature to 0°C. You rush home and close the windows, but the interior temperature has already fallen to 4°C. The temperature-regulating system senses the acute cold load (*step 1a* in Fig. 5*A*). Simultaneously, the system's coordinating center recognizes that low outside temperature has rotated upward the J_{cold}-vs.-T curve (dashed curve and *step 1b* in Fig. 5*A*). Nevertheless, at the temperature of 4°C, J_{heat} greatly exceeds J_{cold}, so that *Eq. 6* predicts that temperature should rise rapidly (*step 2* in Fig. 5*B*). Of course, as the temperature rises, J_{heat} gradually falls and J_{cold} gradually rises (*steps 3a* and *3b* in Fig. 5*B*) until the two eventually come into balance, not at the initial steady-state temperature of 22°C, but at the new steady-state temperature of 17°C, as dictated by the intersection of the J_{heat}-vs.-T curve and the newly rotated J_{cold}-vs.-T curve.

This is an example of a compound temperature-control perturbation: an acute cold load complicated by a chronic increase in J_{cold}. As illustrated in Fig. 5*C*, the blast of cold air through the left-open windows causes a sudden temperature fall, and the temperature-control system causes the temperature to recover, but only partially. Does this difference between the initial and final steady-state temperatures mean that the temperature-control system failed? No. The system performed precisely as designed, causing the temperature to recovery to as high a value as it possibly could have, given the kinetic parameters that we designed into the system. In particular, *temperature regulation* in Fig. 5*C* was rather good, as indicated by the rate of temperature recovery from the acute cold load.

Similar compound perturbations commonly occur in the world of pH_i regulation. As an example, consider respiratory

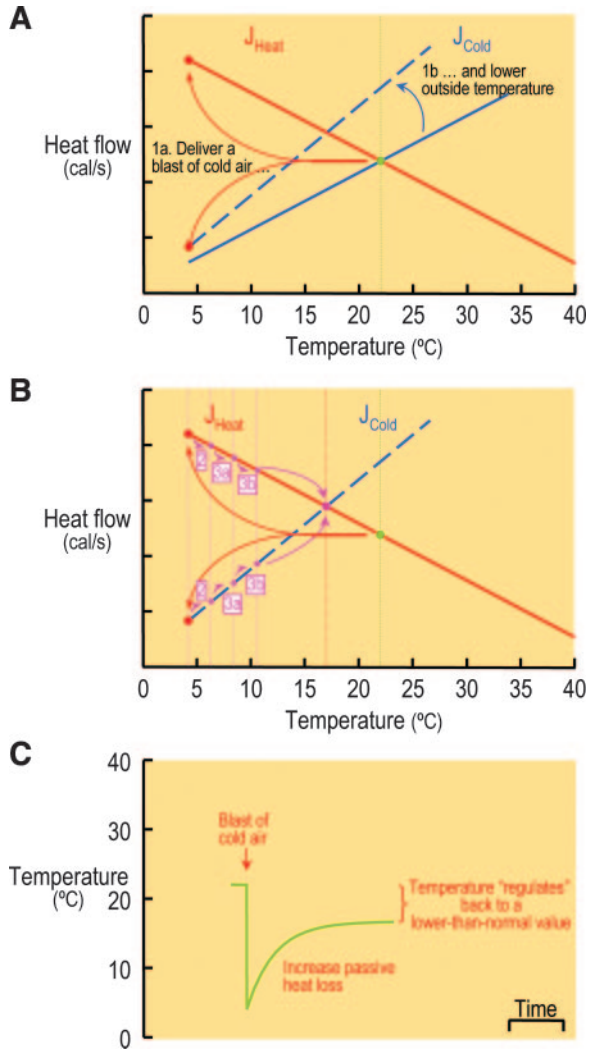

Fig. 5. Response to a compound perturbation: an acute cold load and a chronic increase in J_{cold}. *A*: dependence of J_{heat} and J_{cold} on temperature. In this example, we apply two thermal insults simultaneously, a blast of cold air (*step 1a*) and an increase in nonregulatory chronic cold loading (dashed line). Thus the compound perturbation is a combination of the insults in Fig. 2, *A* and *B*, and in Fig. 4. *B*: changes in J_{heat} and J_{cold}. Immediately after the increase in J_{cold}, J_{cold} greatly exceeds J_{heat} (*step 2*), so that temperature initially recovers rapidly. As temperature rises, the difference between J_{heat} and J_{cold} decreases (*steps 3a* and *3b*), until the two values eventually come into balance at a temperature of 17°C. *C*: time course of temperature. At any instant in time, the rate of the temperature recovery is proportional to the difference ($J_{heat} - J_{cold}$). If the heat capacity had been doubled in this example, the magnitude of the initial decrease temperature would have been only half as great as shown in the figure. However, the final steady-state temperature would be the same.

acidosis, in which a rise in extracellular $[CO_2]$ causes extracellular pH to fall. The rise in $[CO_2]$ leads to an influx of CO_2 and thus an *acute* intracellular acid load. The fall in extracellular pH_o inhibits acid extruders and stimulates acid loaders and thus causes a chronic intracellular acid load.

One way to quantify the ability of our temperature-control system to maintain a stable steady-state interior temperature in the face of an altered exterior temperature would be to define a parameter called *temperature stability* or $\Delta T_i/\Delta T_o$—the change in steady-state interior temperature for an imposed change in exterior temperature. Later, we will discuss a similar definition in the domain of acid-base physiology.

An important lesson that we learned from Figs. 3–5 is that an isolated change in kinetics that affects the value of *either* J_{heat} *or* J_{cold} at the original steady-state temperature will always cause the steady-state temperature to change. We could draw a comparable conclusion concerning steady-state pH_i. Of course, it is possible for coordinated change in both J_{heat} and J_{cold} to leave the steady-state temperature unaltered. In this case, the intersection of the old J_{heat}-vs.-T and old J_{cold}-vs.-T curves would occur at the same temperature (but not the same energy flux) as the intersection of the new J_{heat}-vs.-T and new J_{cold}-vs.-T curves—as we shall see in the next section.

Environmental Sensors

The experiment in Fig. 5 revealed a flaw in our temperature-control system: environmental changes may lead to a change in steady-state temperature. We might compensate for the flaw by introducing one or more environmental sensors that warn the coordinating center of impending changes in the unregulated components of J_{heat} and/or J_{cold}.

Environmental temperature. The most obviously useful environmental sensor might be one that detects changes in exterior temperature (T_o). For example, we could program our temperature-regulating system to respond to a decrease in T_o by increasing the output of the furnace and/or decreasing the output of the air conditioner. Such a T_o-dependent shift in the temperature-sensitivity of a furnace could counteract the shift in steady-state temperature that we saw in Fig. 5*C*. However, we will underplay this type of sensor inasmuch as there is presently no evidence that the analogous pH_o sensors play a role in coordinating pH_i regulation. Sensors for pH_o clearly exist. For example, vascular smooth muscle cells dilate in response specifically to a fall in pH_o (2, 3). In sensory neurons the acid sensing ionic channel, which is primarily permeable to Na^+, mediates a fast-rising and desensitizing inward current when pH_o falls below 6.9 (25, 46). Other examples of pH_o-sensitive channels are the tandem pore-domain acid-sensitive K^+ channels, which are inhibited by decreases in both pH_o and pH_i below values of ~7.3, and the human pancreatic tandem-pore K^+ channel, which is stimulated at pH_o values >7.4 and inhibited by pH_o values <7.4 (22, 26, 30).

Snow sensors. Whereas a T_o sensor would provide direct information about a key parameter that directly influences unregulated J_{heat} and J_{cold}, a snow sensor would provide information about a parameter that is associated with increased passive heat loss. We might program the coordinating center to respond to the appearance of snow by increasing the output of the furnace over a range of temperatures, and by decreasing the output of the air conditioner, as shown in Fig. 6*A*. With these modifications, the system might appropriately detect the approach of a blizzard and prevent the house temperature from falling. As we will see later, an analogous sensor in cells might detect extracellular CO_2 and signal certain cells to stimulate acid-base transporters.

Sun sensors. A sun sensor would provide information about a parameter that is associated with passive heat gain. By programming the coordinating center to respond to increased sunlight by increasing the output of the air conditioner at each temperature, and by decreasing the output of the furnace (Fig. 6*B*), we might appropriately compensate for the increasing heat loads that often accompany a sunny day. As we will see later, an analogous sensor in cells might detect extracellular HCO_3^-, and in response to *decreases* in extracellular levels of this ion, may signal certain neurons to enhance acid extrusion and/or inhibit acid loading.

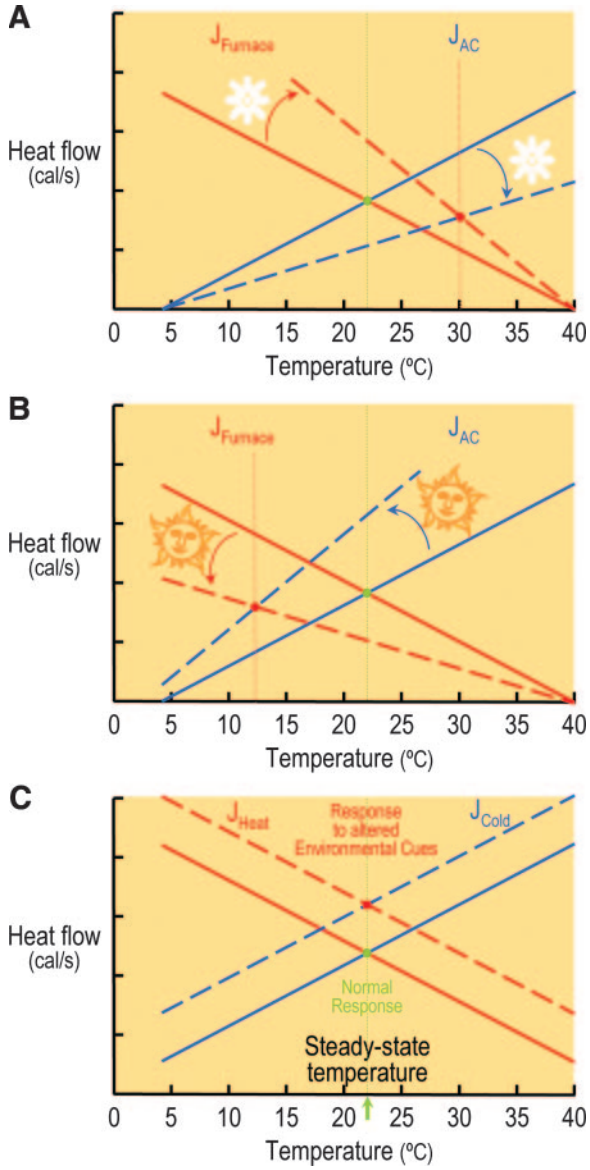

Fig. 6. Environmental sensors. *A*: a snow sensor. In this example, a detector sensing snow stimulates the furnace but inhibits the air conditioner. *B*: a sun sensor. In this example, a detector sensing an increase in sunlight inhibits the furnace but stimulates the air conditioner. *C*: hypothetical response of the overall J_{heat}-vs.-temperature and J_{cold}-vs.-temperature relationships to altered environmental cues. For example, although a blizzard might raise J_{cold}, the environmental sensors might trigger a compensatory increase in J_{heat} so that the steady-state temperature would remain unaffected.

Integrated responses to environmental sensors. Of course, we might wish to provide additional data concerning such relevant environmental parameters as wind speed. Even more important, we might wish to program the coordinating center to integrate appropriately information on all of the environmental parameters so that it would respond intelligently to a mixed message–such as those provided by bright sunlight when the

exterior temperature is −30°C. In the ideal situation, our temperature-control system would respond to varying environmental cues by fine tuning the J_{heat}-vs.-T and J_{cold}-vs.-T relationships so that they always intersected at the target temperature of 22°C (Fig. 6*C*). As we will see later, when certain neurons are challenged by metabolic acidosis–a fall in extracellular pH caused by a decrease in the extracellular HCO_3^- concentration at a fixed level of CO_2–they are somehow able to maintain a near-stable pH_i.

Overview of pH_i Homeostasis

The foregoing discussion, in which we treated the problem of pH_i regulation as if it were a problem in temperature regulation, is very likely to be true a century from now. The discussion that follows, in which we examine pH_i regulation per se, necessarily will be less complete and more tentative. It will be less complete because cells use many different transporters as the analogs of furnaces and air conditions, and because different cell types make use of different subsets of these transporters. Our pH_i discussion will be more tentative than our temperature discussion because I am not aware of a single cell type for which, as of this writing, we know at the molecular level just which transporters make which contribution to pH_i homeostasis. Moreover, we are only beginning to understand the regulation of individual transporters and the interactions among them. Thus much of what one might write today about the *details* of pH_i regulation will be outdated a year or a decade from now. However, our discussion of temperature regulation has laid the groundwork for understanding the fundamental *concepts* of pH_i regulation, and these concepts will likely withstand the test of time.

Thus far we mentioned the word "pH"—and associated acid-base terms—only parenthetically. Nevertheless, if you understand the concepts that we have developed in our discussion of temperature regulation, then you understand the principles necessary for being a midlevel expert in the field of pH_i regulation. You merely must change the names of the terms we have been using: replace temperature with pH, heat capacity with buffering power, cold loading with acid loading, furnace with acid extruder, and so on.

pH is defined as the negative logarithm (base 10) of the H^+ activity (a parameter that measures the effect that the ion produces, which is usually less than its actual concentration). If we make the simplifying assumption that the H^+ concentration is the same as activity

$$pH = -\log_{10}[H^+] \quad (7)$$

The pH scale is a scale of ratios. Because the $\log_{10}$ of 10 is 1 and the $\log_{10}$ of 2 is ~0.3, tenfold changes in $[H^+]$ correspond to pH changes of 1 and twofold changes in $[H^+]$ correspond to pH changes of ~0.3.

Buffering (Heat Capacity)

Buffers. According to Brønsted's definition, an acid is any substance that is capable of donating a proton. In the general sense

$$HB^{(n+1)} \rightleftarrows B^{(n)} + H^+ \quad (8)$$

where n is the valence. In this example, $HB^{(n+1)}$ is a weak acid, and $B^{(n)}$ is its conjugate weak base.[1] Viewed differently, $B^{(n)}$ is a weak base, and $HB^{(n+1)}$ is its conjugate weak acid. Other common examples of weak acids include ammonium (NH_4^+), carbonic acid (H_2CO_3), and monobasic inorganic phosphate ($H_2PO_4^-$):

$$NH_4^+ \rightleftarrows NH_3 + H^+$$
$$H_2CO_3 \rightleftarrows HCO_3^- + H^+ \quad (9)$$
$$H_2PO_4^- \rightleftarrows HPO_4^= + H^+$$

The corresponding conjugate weak bases are NH_3, HCO_3^-, and dibasic inorganic phosphate $HPO_4^=$. For each of these buffers, the equilibrium is described by an equation of the form:

$$K = \frac{[B^{(n)}] \cdot [H^+]}{[HB^{(n+1)}]} \quad (10)$$

where K is the equilibrium constant. In its logarithmic form, the relationship becomes:

$$pH = pK + \log_{10}\frac{[B^{(n)}]}{[HB^{(n+1)}]} \quad (11)$$

where pK is $-\log_{10}K$. Thus when pH = pK (i.e., when $[H^+] = K$), $[B^{(n)}] = [HB^{(n+1)}]$.

We could write a similar equation for the CO_2/HCO_3^- buffer system:

$$pH = pK + \log_{10}\frac{[HCO_3^-]}{[CO_2]} \quad (12)$$

The concentration of dissolved CO_2 is given by Henry's law,

$$[CO_2] = s \cdot P_{CO_2} \quad (13)$$

where s is the solubility of CO_2 (in mM/mmHg) and P_{CO_2} is the partial pressure of CO_2 in the gas phase with which the aqueous solution is in equilibrium. Combining *Eq. 12* and *Eq. 13* yields the Henderson-Hasselbalch equation:

$$pH = pK + \log_{10}\frac{[HCO_3^-]}{s \cdot P_{CO_2}} \quad (14)$$

Buffering power. Together, a weak acid and its conjugate weak base constitute a *buffer pair*. That is, the members of the buffer pair are capable of reversibly releasing or binding a proton, and thereby acting as a buffer. *Buffering power* (β) is defined as the amount of strong base (e.g., NaOH)—or the negative of the amount of strong acid (e.g., HCl)—that one would have to add to a liter of solution to raise the pH of the solution by 1 pH unit:

$$\beta \equiv \frac{\Delta\text{Strong Base}}{\Delta pH} = -\frac{\Delta\text{Strong Acid}}{\Delta pH} \quad (15)$$

The amount of strong acid or strong base is generally given in millimoles. Strictly speaking, pH is unitless, so that it is

[1] A weak acid or base is one that is not necessarily fully dissociated. For example, HCl is a strong acid because it is virtually fully dissociated into H^+ and Cl^-.

correct to give buffering power in units of mM. However, authors often explicitly include pH: mM/pH unit. This designation has the advantage of making it easier to keep track of units in complex calculations.

Buffering in a closed system. As it happens, buffering power varies with pH. How might we measure the pH dependence of buffering power? In this example, we will work with a *closed-system buffer*, that is, one in which neither member of the buffer pair can escape from (or be added to) the beaker either by equilibrating with the atmosphere or by some biochemical or transport reaction. Inorganic phosphate or HEPES would be such a buffer. For simplicity, let us assume that the buffer has a pK of 7. We will start with a beaker of buffer solution at a pH of, say, 4. We will now add a small amount of NaOH (i.e., ΔStrong Base in *Eq. 15*). The added OH^- will have two fates: (1) Some will be neutralized (i.e., buffered) as $HB^{(n+1)}$ dissociates into $B^{(n)}$ and H^+, and the H^+ then combines with the OH^- to form H_2O; this sequence of reactions will result in no pH change (2). The rest of the added OH^- will equilibrate with H^+ and H_2O and thereby raise the pH of the solution by a small amount (i.e., ΔpH in *Eq. 15*), raising the pH to slightly more than 4. We then use *Eq. 15* to compute the mean β over the pH range 4 − (4 + ΔpH). We plot this computed β in Fig. 7*A* at the mean pH of 4 + ΔpH/2, and repeat the whole procedure many times as the computed β rises to a maximum at a pH of 7 and then falls to near-zero values as we approach a pH of 10.

This experiment demonstrates that, in a closed system, the maximal buffering power occurs when pH equals pK. We could reach this same conclusion mathematically by realizing that the amount of buffered OH^- equals $\Delta[B^{(n)}]$, and that

$$\beta \equiv \frac{\Delta\text{Strong Base}}{\Delta\text{pH}} \cong -\frac{\Delta[B^{(n)}]}{\Delta\text{pH}} \qquad (16)$$

If we would combine *Eq. 10* and *Eq. 16*, and then take the partial derivative of $B^{(n)}$ with respect to pH (holding the amount of total buffer constant), we would see that

$$\beta_{closed} = 2.3 \cdot [TB] \frac{[H^+] \cdot K}{([H^+] + K)^2} \qquad (17)$$

Here, [TB] is $[HB^{(n+1)}] + [B^{(n)}]$, the total buffer concentration. If we would plot β_{closed} as a function of pH, we would obtain the bell-shaped curve in Fig. 7*A*. The maximal β_{closed} is 58% of [TB].

Buffering powers are additive, so that if we had a solution containing a mixture of many closed-system buffers, we could simply add their individual buffering powers to obtain the total buffering power of the solution. In the example of Fig. 7*B*, the hypothetical solution consists of nine buffers, each at a concentration of 1 mM, with their pK values evenly spaced at intervals of 0.5. Note that in the center of this pH range, the total buffering power is remarkable constant. Indeed, the total closed-system buffering power of cells is remarkably constant over a wide pH range, tending to fall gradually as pH_i rises. Thus the relative constancy of β_{closed} in a cell is not terribly different from the absolute constancy of heat capacity in our house.

Buffering in an open system. Although the foregoing analysis works quite well for most buffers, it fails badly when [TB] is not constant. The most common example in which [TB] is not constant is the CO_2/HCO_3^- buffer pair, where the volatile CO_2 freely exchanges with its environment. In this case, $[CO_2]$ is constant, but [TB] can vary over a very wide range. Open-system buffering by CO_2/HCO_3^- is extremely important in pH_i regulation because we can generally regard the extracellular solution as an infinite sink for CO_2, which can freely diffuse across most cell membranes. Thus we can generally regard $[CO_2]_i$ as fixed.

Imagine an experiment in which we begin with a beaker that contains one liter of an aqueous solution that—in terms of CO_2/HCO_3^- and pH—mimics mammalian blood plasma (Fig. 8). However, the beaker contains no other buffers. The atmosphere has a P_{CO_2} of 40 mmHg, the dissolved $[CO_2]$ is 1.2 mM (as determined by Henry's law), the pH of the solution is 7.4, and $[HCO_3^-]$ is 24 mM. We now add 10 mmol of HCl to the beaker (two panels at top right). Nearly all of the added 10 mmol of H^+ are neutralized as they combine with nearly 10 mmol of HCO_3^- to form nearly 10 mmol of H_2CO_3, which in turn forms nearly 10 mmol of CO_2. The excess CO_2 evolves into the atmosphere so that the final $[CO_2]$ is the same as the initial $[CO_2]$. Because the buffering reaction is not limited by the buildup of the ultimate reaction product (i.e., CO_2), buffering is quite effective, and pH falls by only ~0.23 (i.e., from 7.40 to 7.17). If we had instead performed this same experiment in a closed bottle, the newly formed CO_2 would not have been able to escape the aqueous solution, the reaction product would have limited the extent of the overall buffer reaction, and pH would have fallen by a substantially greater amount.

The two panels at the lower right of Fig. 8 illustrate a hypothetical experiment similar to the previous one, but in which we add 10 mM of NaOH to the beaker. In this case, CO_2 and H_2O combine to form H_2CO_3, which in turn dissociates to form HCO_3^- and the H^+ which neutralizes almost all of the added OH^-. At the beginning of the experiment, the beaker

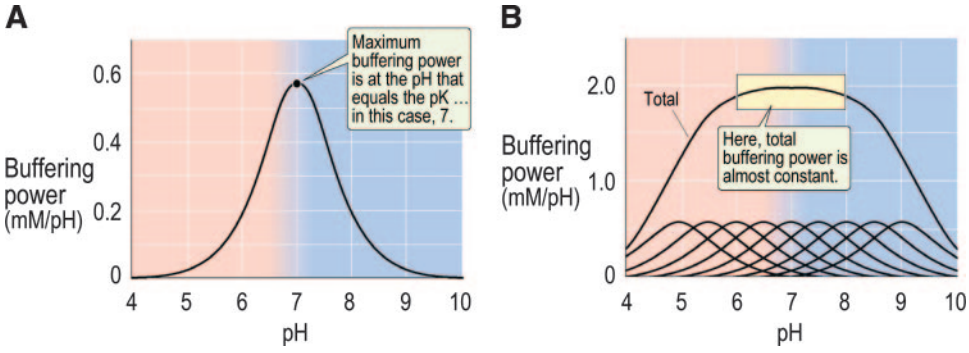

Fig. 7. The pH dependence of buffering power in a closed system. *A*: single buffer. in a closed system. *Equation 17* was used to compute buffering power, assuming a pK of 7 and a total buffer concentration of 1 mM. *B*: multiple buffers in a closed system. The nine lower curves were each computed using *Eq. 17*. In each case, the total buffer concentration was 1 mM; pK values ranged from 5.0 to 9.0 in steps of 0.5. The center curve is the same as in *A*. The upper curve is the sum of the nine lower curves. Reproduced by permission of Elsevier (5).

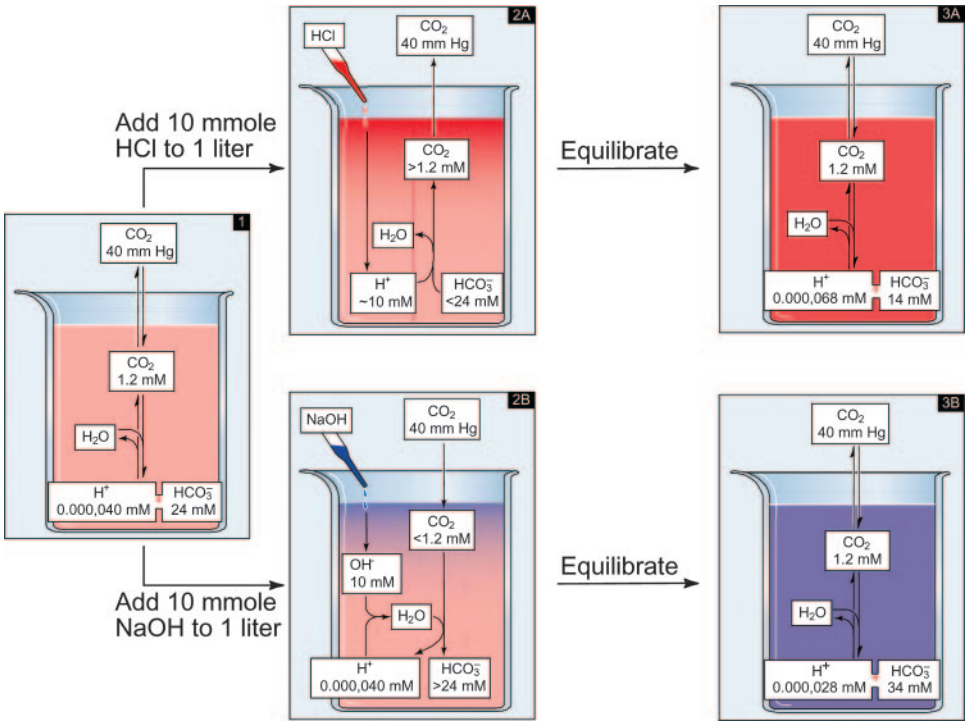

Fig. 8. Buffering in an open system. The beaker of the left (*step 1*), which contains 1 liter of solution having a pH of 7.4, represents the starting conditions. The two beakers at the top represent the effect of adding 10 mM of HCl. As HCO_3^- neutralizes the added H^+ (*step 2A*), $[HCO_3^-]$ falls and $[CO_2]$ rises. The latter leads to the net diffusion of CO_2 from the beaker. After nearly all of the added 10 millimoles of H^+ have been buffered by HCO_3^-, the system is once again in equilibrium (*step 3A*), with a pH of 7.17 and a $[HCO_3^-]$ of 14 mM. The two beakers at the bottom represent the effect of adding 10 millimoles of NaOH. As CO_2 and H_2O form HCO_3^- and H^+, the newly formed H^+ can neutralize the added OH^- (*step 2B*), forming H_2O. As a result $[HCO_3^-]$ rises and $[CO_2]$ falls. The latter leads to the net diffusion of CO_2 from the atmosphere into the beaker. After nearly all of the added 10 mM of OH^- have been buffered by CO_2, the system is once again in equilibrium, with a pH of 7.55 and a $[HCO_3^-]$ of 34 mM. Reproduced by permission of Elsevier (5).

contained only 1.2 mM of CO_2. Yet the buffering reaction consumed nearly 10 mM of CO_2. This was possible because CO_2 from the atmosphere dissolved in the solution to replenish the consumed CO_2. At the end of the experiment, the $[CO_2]$ concentration is the same as at the beginning, and the pH of the solution has risen by only 0.15 (i.e., from 7.44 to 7.55).

If we were to repeat the experiments in Fig. 8, but add much smaller amounts of HCl or NaOH, we could compute the pH dependence of the CO_2/HCO_3^- buffer system over a wide pH range. The steadily rising curve in Fig. 9 shows the result of such series of hypothetical experiments. If we would combine *Eq. 10* and *Eq. 16*, and then take the partial derivative $B^{(n)}$ with respect to pH, holding $[CO_2] = [HB^{(n+1)}]$ constant, we would see that

$$\beta_{open} = 2.3 \cdot [HCO_3^-] \quad (18)$$

Because at a fixed P_{CO_2} $[HCO_3^-]$ rises exponentially with pH, β_{open} also rises exponentially with pH. Thus the pH dependence of β_{open} is strikingly different from the temperature dependence of heat capacity (which is *not* temperature dependent). Because of the open-system CO_2/HCO_3^- buffering power, cells become increasingly resistant to changes in pH_i as pH_i increases.

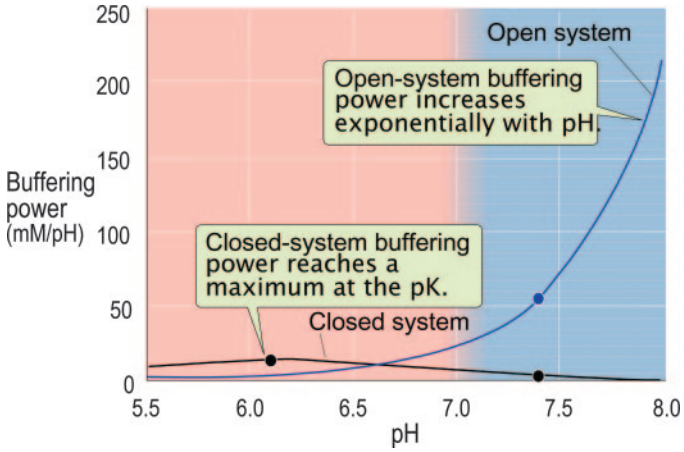

Fig. 9. The pH dependence of buffering power in an open system. *Equation 18* was used to compute the open-system buffering power, assuming a pK of 6.1 and a $[CO_2]$ of 1.2 mM. *Equation 17* was used to the compute closed-system buffering power, assuming that the system was closed at a pH of 7.4, when $[HCO_3^-]$ was 24 mM and $[CO_2]$ was 1.2 mM. Reproduced by permission of Elsevier (5).

The flattened, bell-shaped curve in Fig. 9 shows what the buffering power of the CO_2/HCO_3^- system would be if we put the starting solution from Fig. 8 into a closed glass bottle. The β_{closed} for CO_2/HCO_3^- is maximal at the overall pK of the CO_2/HCO_3^- equilibrium, 6.1.

Total buffering power in a cell. The buffering power that is most relevant for a cell is that of the cytosol–the compartment in direct contact with the plasma membrane and most other membrane–enclosed cellular compartments. The total intracellular buffering power is the sum of the individual buffering powers of all cytosolic buffers, regardless of whether they behave as closed- or open-system buffers. These cytosolic buffers generally can be divided into two classes. The *intrinsic buffers* are the closed system buffers, the aggregate buffering power of which one would measure experimentally (36). The *extrinsic buffers* are the open-system buffers, like the CO_2/HCO_3^- buffer pair, that one has the option of adding to the system. In principle, these extrinsic buffers could be any buffer pair in which one of the members could readily cross the cell membrane. Examples might include butyrate/butyric acid (the neutral weak acid is often permeant) and NH_3/NH_4^+ (the neutral NH_3 is generally permeant). One computes the buffering power of these open-system buffers using an expression

analogous to *Eq. 18*. In mammalian cells (exposed to a P_{CO_2} of 40 mmHg), the open-system CO_2/HCO_3^- buffering power accounts for one-half to two-thirds of the total buffering power at the resting pH_i. Of course, the total intracellular buffering power, as well as the contribution of CO_2/HCO_3^-, increase at higher pH_i values.

Perturbations: Acute and Chronic Acid and Alkali (Heat/Cold) Loads

Acute acid and alkali loads: microinjection. In the laboratory, one can acutely acid load a cell by injecting or iontophoresing H^+ into the cytosol, as was pioneered by Roger Thomas (42). Figure 10*A* illustrates a hypothetical experiment in which we microinject HCl into a cell. For the sake of simplicity, we will assume that the cell is bathed in a solution that does not contain any CO_2/HCO_3^-. Thus only closed-system non-HCO_3^- buffers will neutralize the injected H^+. The minute amount of injected H^+ that does not react with $B^{(n)}$ causes intracellular pH to fall.

Conversely, if we microinject KOH into a cell (Fig. 10*B*), non-HCO_3^- buffers will provide the H^+ to neutralize almost all of the injected OH^-. The minute amount of unbuffered OH^- is responsible for the observed pH_i increase. Typically, cellular buffers will neutralize more than 99.99% of the H^+ or OH^- presented to them.

Acute acid and alkali loads: permeant weak acids and bases. Although the hypothetical experiments in Fig. 10 nicely illustrate the concept of imposing an acute acid or alkali load, microinjections are only possible in a laboratory setting and require not only a skilled experimenter but a large cell. As illustrated in Fig. 11*A*, a far easier way to acid load a cell-and one to which cells are regularly subjected in vivo-is to increase the concentration of CO_2 in the extracellular fluid (8). CO_2 crosses the plasma membranes of most cells very easily. Once in the cytosol, the CO_2 can combine with H_2O to form H_2CO_3, most of which (but not all) then very slowly dissociates to form HCO_3^- and H^+. Most cells contain abundant *carbonic anhydrase*, an enzyme that in effect catalyzes the conversion of $CO_2 + H_2O$ to H_2CO_3 and thus accelerates the acidification of the cell. Almost all the H^+ formed in this reaction sequence is buffered by non-HCO_3^- buffers. Note that the CO_2/HCO_3^- buffer pair cannot buffer the H^+ produced by the influx of CO_2. In this experiment, we are assuming that the cell has no pH_i regulatory mechanism. Thus the influx of CO_2 causes pH_i to fall and then level off once $[CO_2]_i$ has risen to the level of $[CO_2]_o$ and the net influx of CO_2 has stopped. When we remove the CO_2, pH_i returns to its initial value. Although we used CO_2 as the permeant weak acid in this experiment, we could have used any permeant weak acid (e.g., acetic acid, butyric acid) to acid load the cell. The extent of the pH_i decline in such an experiment depends on the intracellular buffering power (greater values of β reduce the magnitude of the pH_i decrease), the initial extracellular concentration of the weak acid, and the relationship between pH_i and the pK of the buffer (the higher the pH_i, and the lower the pK, the greater the net acidification).

Figure 11*B* illustrates a hypothetical experiment in which we use a permeant weak base to alkali load the cell. The most widespread permeant weak base used in the laboratory is NH_3, and indeed the influx of NH_3 into certain renal tubule cells is important for the renal handling of NH_3/NH_4^+. In addition, the influx of NH_3 into cells throughout the body can be important during liver failure (when levels of NH_3 rise). As shown in Fig. 11*B*, when $[NH_3]_o$ exceeds $[NH_3]_i$, NH_3 enters the cell and combines with protons that are provided by buffers other than NH_3/NH_4^+. If no other transport processes are at work, and if the cell is incapable of regulating pH_i in response to this acute alkali load, then the exposure to NH_3 will cause pH_i to rise to a new stable pH_i once $[NH_3]_i$ has risen to the level of $[NH_3]_o$. Returning the extracellular $[NH_3]_o$ to its original value in this example

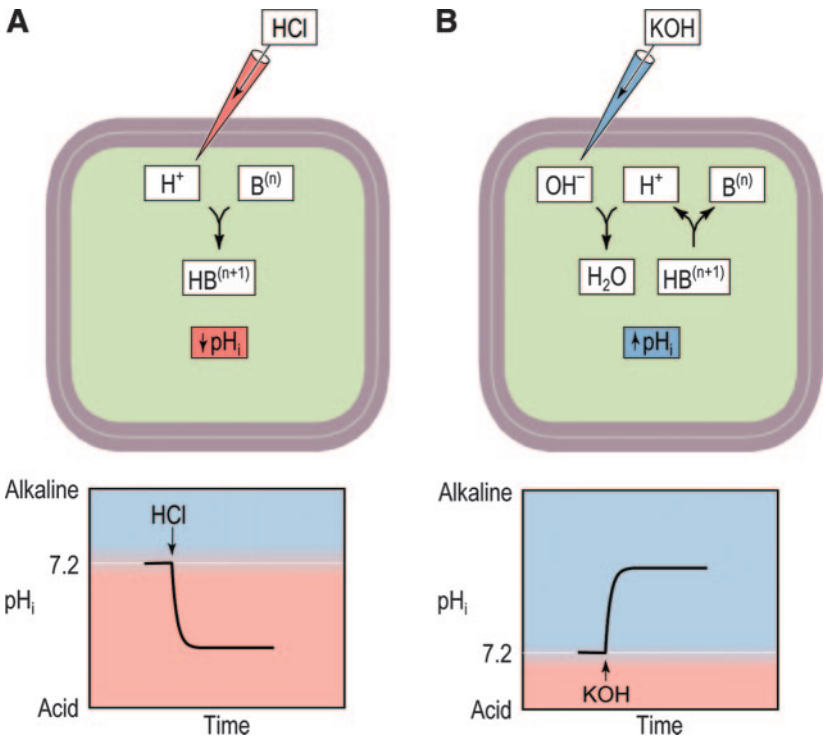

Fig. 10. Acute acid and alkali loads produced by microinjection. *A*: microinjection of HCl. $B^{(n)}$ and $HB^{(n+1)}$ represent non-HCO_3^- buffers. If CO_2 and HCO_3^- were also present, then HCO_3^- would compete with $B^{(n)}$ for the injected H^+ according to the reactions in Fig. 8/*step 2A*. In this case, the total buffering power would be greater, and the intracellular pH (pH_i) decrease would be smaller. The bottom panel shows that, in the absence of acid-base transporters, pH_i would be stable after its initial decline. *B*: microinjection of KOH. If, in addition to the non-HCO_3^- buffer, CO_2 and HCO_3^- were also present, then CO_2 would compete with $HB^{(n+1)}$ for the injected OH^- according to the reactions in Fig. 8/*step 2B*.

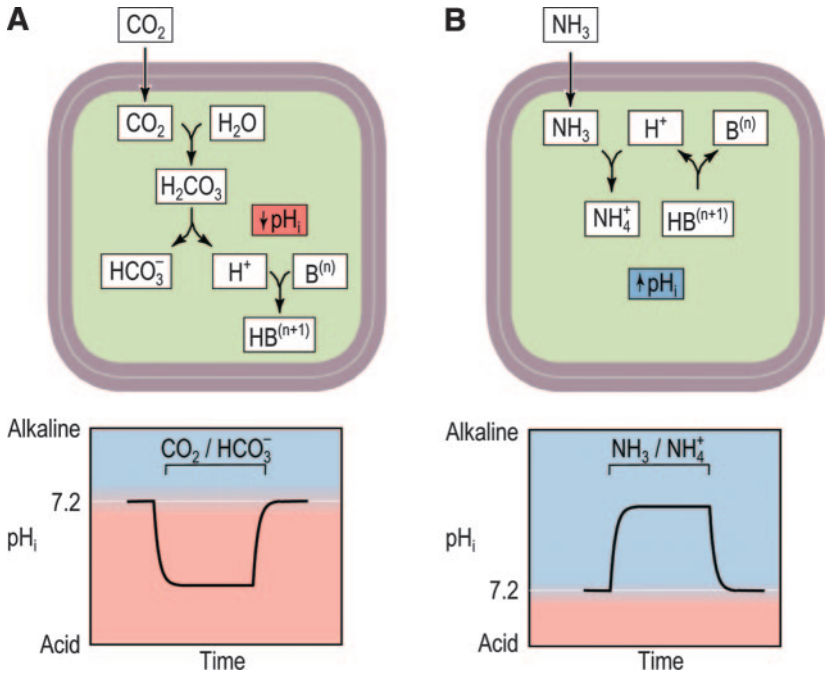

Fig. 11. Acute acid and alkali loads produced by exposing the cell to a permeant weak acid or weak base. *A*: exposure to a permeant weak acid. In this case, CO_2 crosses the plasma membrane, ultimately producing H^+. Non-HCO_3^- buffers neutralize almost all of the newly produced H^+, thereby minimizing the pH_i decrease. The bottom panel shows that, in the absence of acid-base transporters, pH_i would be stable after its initial decline, and would return to precisely its original value after the removal of CO_2/HCO_3^-. *B*: exposure to a permeant weak base. In this case, NH_3 crosses the plasma membrane, consuming H^+. Non-HCO_3^- buffers provide almost all of the H^+ needed for the formation of NH_4^+, thereby minimizing the pH_i increase. If CO_2/HCO_3^- were present, CO_2 would also provide H^+, according to the reactions in Fig. 8/*step 2B*.

will cause pH_i to return to its original value as well. Instead of using NH_3, we could have used other permeant weak bases, such as methylamine. Note that many pharmacological agents with amine groups behave as permeant weak bases.

Once added to a cell, CO_2 and NH_3 behave as open-system buffers, and augment the total buffering power of the cell. Although the CO_2/HCO_3^- system cannot buffer the protons produced as CO_2 enters the cell in Fig. 11*A*, the CO_2/HCO_3^- system could buffer the NH_3 that enters the cell in Fig. 11*B*. The same is true in reverse for the NH_3/NH_4^+ buffer system.

Chronic acid and alkali loads: passive fluxes across the plasma membrane. The equilibrium (or Nernst) potential for H^+ (E_H) is the hypothetical membrane potential at which H^+ would be in equilibrium across the membrane. According to the laws of electrochemistry

$$E_H = \frac{2.3\ RT}{F} \cdot \log_{10}\left(\frac{[H^+]_o}{[H^+]_i}\right) \qquad (19)$$

where $[H^+]_o$ is the extracellular H^+ concentration, $[H^+]_i$ is the intracellular $[H^+]$, and R, T, and F have their usual meanings. Figure 12 illustrates how we might compute E_H when the relevant values are reasonably physiological: pH_i is 7.2, pH_o is 7.4, and the transmembrane voltage (V_m) is −60 mV. Under these conditions, E_H is −12 mV. In other words, if V_m were −12 mV, no energy would be required or released to move H^+ across the membrane in either direc-

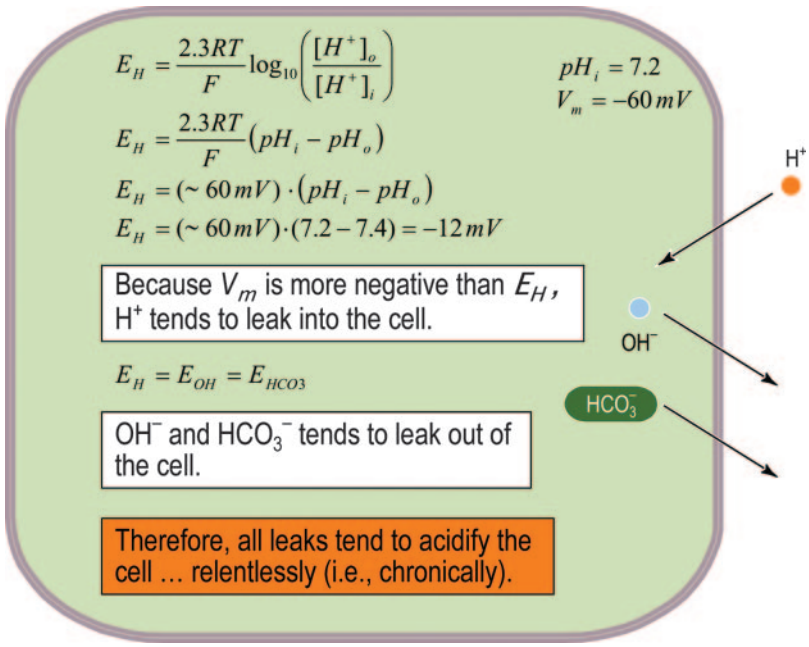

Fig. 12. Chronic acid and alkali loads produced by passive fluxes of charged weak acids and bases across the plasma membrane. In this example, we assume that the cytosolic pH is 7.2 and that the transmembrane voltage is −60 mV.

tion. Because V_m is in fact −60 mV in this example, the voltage inside the cell is far too negative for H^+ to be in equilibrium. As a result, protons tend to enter the cell passively down their electrochemical gradient. This influx of H^+ is in principle never ending. As long as the gradient for H^+ remains inward, and as long as the cell membrane remains permeable to H^+, protons will enter the cell passively, imposing a chronic intracellular acid load.

It is possible to show that the equilibrium potential for OH^- (E_{OH}) is identical to that for H^+. Moreover, if the concentration of CO_2 (or any neutral weak acid) is the same on both sides of the membrane, then $EHCO_3$ (or the equilibrium potential for the conjugate weak base) also will be the same as E_H. Finally, if the concentration of NH_3 (or any neutral weak base) is the same on both sides of the membrane, then ENH_4 (or the equilibrium potential for the conjugate weak acid) also will be the same as E_H. That is

$$E_H = E_{OH} = E_{HCO_3} = E_{NH_4} \quad (20)$$

Because V_m is more negative than ENH_4, the positively charged NH_4^+-like H^+-will tend to passively enter the cell. Conversely, because V_m is more negative than E_{OH} and $EHCO_3$, the negatively charged OH^- and HCO_3^- will tend to passively exit the cell. All of these movements tend to impose a chronic intracellular acid load. Harkening back to our temperature-regulation model, these passive fluxes are akin to heat escaping from our house during the winter. The lower the pH_o (the lower outside temperature), the greater the tendency for acid to accumulate inside the cell (the faster the house loses heat).

Regulation: acid extruders and loaders (furnaces and air conditioners). Just as the house in our temperature-regulation analogy had a furnace and an air conditioner to regulate temperature, cells have a host of acid-base transporters that perform analogous functions. The so-called *acid extruders*—which are analogous to furnaces—use energy to extrude H^+ from the cell or to accumulate a weak base, such as HCO_3^-. Just as a furnace raises temperature, an acid extruder raises pH_i. We quantify the rate of acid extrusion (J_E), analogous to J_{heat}, as the rate at which acid equivalents exit the cell per volume of cell water, or per surface area of cell membrane. Because the membrane surface area is usually difficult to measure, most investigators report J_E in units such as μM/s. Experimentally, one obtains J_E as the product of the rate of pH_i recovery (dpH_i/dt) at a particular pH_i value by the total intracellular buffering power (β) at that same pH_i. This calculation would be analogous to obtaining J_{heat} as the product of dT/d*t* (the rate of temperature change) and C (the heat capacity).

The so-called *acid loaders*—which are analogous to air conditioners—mediate the passive exit of weak bases—generally HCO_3^- or $CO_3^=$. Just as an air conditioner lowers temperature, an acid loader lowers pH_i. The rate of acid loading (J_L) is analogous to J_{cold}. The analogy between air conditioners and acid loaders breaks down somewhat because, whereas air conditioners require the input of energy, acid loaders at least in theory work without the direct input of energy. It is perhaps also worth noting that certain acid-base transporters can—at least under some experimental conditions—switch their direction of net transport if the gradient driving transport reverses. This situation would be somewhat analogous to using a heat pump to, alternately, heat and cool our house.

Acid extruders. The acid extruders are listed on the left side of Fig. 13. They all require the input of energy either to extrude H^+ from the cell, or to take up HCO_3^-. The vacuolar-type H^+ pump uses the energy of ATP hydrolysis to extrude H^+ from the cell, whereas the Na/H exchanger uses the energy of the Na^+ gradient to extrude the H^+. The Na/H exchanger was first studied at the cellular level by Murer and colleagues (27), and the first Na/H exchanger was cloned by Pouysségur and colleagues (39). For an overview of the Na/H exchangers (the SLC9 family of transporters), consult the review by Orlowski and Grinstein (28). Several Na^+-driven HCO_3^- (or $CO_3^=$) transporters also are acid extruders. The *Na^+-driven Cl-HCO_3^- exchanger* was first discovered by Thomas in snail neurons (41, 43), and by Russell, De Weer, Roos, and Boron in their work on squid axons (7, 8, 11, 37) and barnacle muscle fibers (4, 9, 10, 38). This was the first transporter ever to be studied as a pH_i regulator. The cDNA encoding a related transporter in *Drosophila* was expression cloned by Romero and colleagues

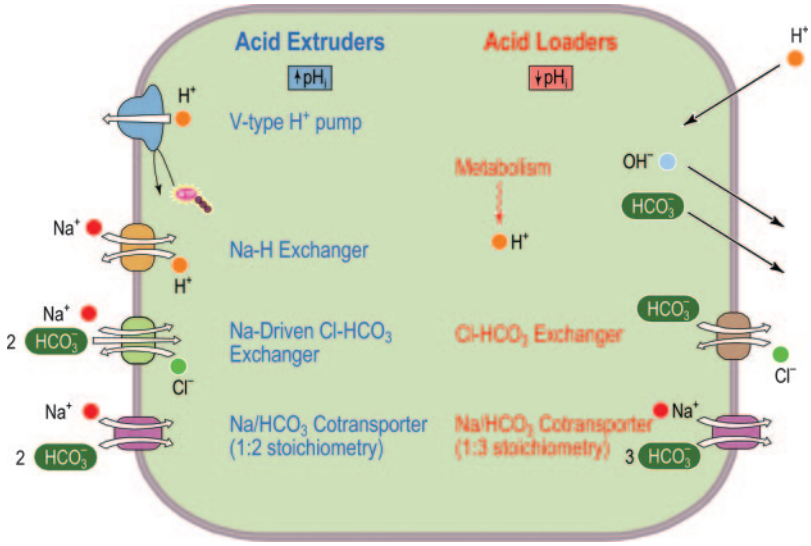

Fig. 13. Acid extruders and acid loaders. Steady-state pH_i depends on the balance between chronic acid extruders and chronic acid loaders. Three of the chronic acid loaders—the passive entry of H^+ and the passive exit of OH^- and of HCO_3^-—are also represented in Fig. 12.

(35), and the gene for the human Na^+-driven Cl-HCO_3 exchanger was cloned by Grichtchenko et al. (20).

The *electrogenic Na/HCO_3 cotransporter* was discovered by Boron and Boulpaep (6) and the gene encoding this transporter (NBCe1) was later cloned by Romero et al. (34). Interestingly, this same protein can either operate with an apparent Na^+:HCO_3^- stoichiometry of 1:2 (in which case it operates as an acid extruder) or, as we will see shortly, with an apparent Na^+:HCO_3^- stoichiometry of 1:3 (in which case it operates as an acid loader). Boron and Boulpaep discovered NBC as it was functioning as an acid loader in the renal proximal tubule. Later, Deitmer and Schlue observed the transporter with similar properties (18), but operating in the 1:2 stoichiometry shown on the left side of Fig. 13.

Not shown in the figure is the third known type of Na^+-coupled HCO_3^- transporter, the electroneutral Na/HCO_3^- cotransporter, the first evidence for which was provided by Aalkjær et al. (1) The cDNA encoding this transporter was cloned by Pushkin et al. (29) and also by Choi et al. (17). The latter group actually showed that the cDNA (NBCn1) encodes an electroneutral Na/HCO_3^- cotransporter that is independent of Cl^-.

Acid loaders. The acid loaders include three nonregulatory mechanisms discussed in connection with Fig. 12–the passive entry of H^+, and the passive exit of OH^- and of HCO_3^-. Figure 13 also shows two HCO_3^- transporters that can act as acid loaders. The *Cl-HCO_3^- exchanger* was the first acid-base transporter ever to be studied in any context. One isoform mediates Cl-HCO_3^- exchanger in erythrocytes. Vaughan-Jones was the first to demonstrate the role of a Cl-HCO_3^- exchanger as an acid loader in the regulation of pH_i (44, 45). The cDNA encoding the erythrocyte transporter (AE1) was cloned by Kopito et al. (24).

We have already mentioned the *electrogenic Na/HCO_3^- cotransporter* in its role as an acid extruder. In renal proximal tubules, the transporter operates with a Na^+:HCO_3^- stoichiometry of 1:3. Given the membrane voltage of proximal-tubule cells, as well as [HCO_3^-] and [Na^+] on either side of the membrane, thermodynamics dictates that the net direction of transport is outward. In the renal proximal tubule, NBCe1 plays a key role in the reabsorption of HCO_3^-. When NBCe1 is expressed in *Xenopus* oocytes, it exhibits a stoichiometry of 1:2. It is not yet clear why NBCe1 has a 1:3 stoichiometry in the proximal tubule. It has been suggested that a novel protein in the proximal tubule complexes with NBCe1 and thereby confers the unusual 1:3 stoichiometry (21). The Cl-HCO_3 exchangers related to AE1 and all the Na^+-coupled HCO_3^- transporters are members of the SLC4 family of transporters. For an overview, consult the review by Romero et al. (33).

Isolating an acid extruder from other elements. In our example of temperature regulation, our house had only one furnace and one air conditioner. Even in such a simple case, it might be difficult to separate the effects of the furnace from the air conditioner because both operate over a rather large, common temperature range. The analysis would be even more challenging if the house had more than one furnace, for example. The situation in cells is indeed more challenging because the typical cell has several acid extruders and several acid loaders. The most straightforward approach for separating out the effects of any one of these would be to acutely load the cell with acid or alkali and then monitor the subsequent recovery of pH_i with and without a specific inhibitor of the transporter in question, an approach first used by Boyarsky et al. (13) to determine the pH_i dependence of the Na/H exchanger in renal mesangial cells.

Consider the model cell in Fig. 14*A*, which has two acid extruders (an H^+ pump and Na/H exchanger) and two acid loaders (an H^+ leakage pathway and the metabolic production of H^+). This cell might very well have several HCO_3^- transporters, but we will minimize their contribution by conducting the experiment in the nominal absence of CO_2/HCO_3^-. The approach (Fig. 14*B*) will be to impose an acute intracellular acid load, using the ammonium prepulse technique (8). Although a detailed description of this approach is outside the scope of this review, the essence is that exposing the cell to a solution containing NH_3/NH_4^+ causes *1*) a rapid pH_i increase due to the influx of the highly permeant NH_3, followed by *2*) a slower acidification due to the uptake of the weak acid NH_4^+, as well as other acid-loading processes. When the NH_3/NH_4^+ is removed, the rapid efflux of NH_3 causes pH_i to plummet to a value well below the initial pH_i, the undershoot reflecting the previous accumulation of NH_4^+ and other acids during the NH_3/NH_4^+ exposure.

If the cell had no pH_i-regulatory apparatus, pH_i would simply fall to a low pH_i and remain there indefinitely (similar to what we modeled in Fig. 11*A*). In the real cell in Fig. 14*B*, however, pH_i rapidly recovered from the acid load. This pH_i

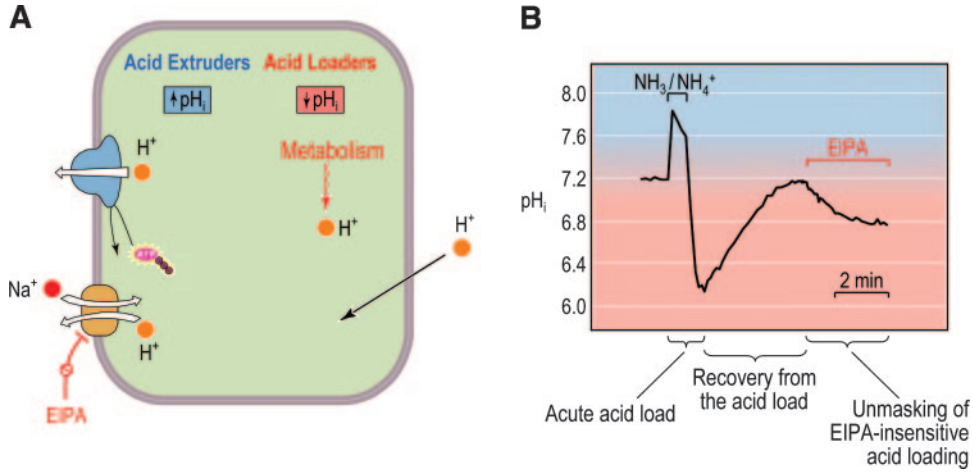

Fig. 14. Recovery of a cell from an acute acid load. *A*: acid extruders and loaders in a model cell. *B*: representative experiment on a single renal mesangial cell. Throughout the experiment, pH_o was 7.40 and temperature was 37°C. During the indicated period, the cell was exposed to a solution containing 20 mM NH_3/NH_4^+. During the indicated period, the cell was exposed to 50 μM ethylisopropyleamide (EIPA) to block Na-H exchange. pH_i was computed from the fluorescence of BCECF. Data in *B* modified from Ref. 13.

recovery is an example of *pH_i regulation* (analogous to our earlier definition of temperature regulation), which we could quantitate as dpH_i/dt or a time constant. When the pH_i reached the pre-NH_3/NH_4^+ value and stabilized, Boyarsky added ethylisopropylamiloride (EIPA), a specific inhibitor of certain isoforms of the Na-H exchanger. The addition of EIPA caused a rather robust acidification. Why? In the steady states that prevailed before the addition of NH_3/NH_4^+ and before the addition of EIPA, the Na/H exchanger was not turned off. Rather, it and other acid extruders were exactly balancing the effect of acid loaders. Blocking the Na/H exchanger unmasked the net acid loading produced by all other acid-base phenomenon other than Na-H exchange. The parallel in our temperature-regulation model would be to block the furnace and watch the temperature fall.

Figure 15 illustrates how we can use the data in experiments similar to that of Fig. 14*B* to determine the pH_i dependence of the Na-H exchanger. As described in Fig. 15, the data in Fig. 15*B* represents the pH_i dependence of the total acid-base flux due to Na-H exchange, including any positive or negative contribution from other processes. The data in Fig. 15*C* represents net acid loading by everything that is *not* Na-H exchange. Finally, Fig. 15*D* represents the pH_i dependence of Na/H exchanger. Although it had previously been thought that the Na/H exchanger turned off at the resting pH_i, these data demonstrate that–like the furnace in

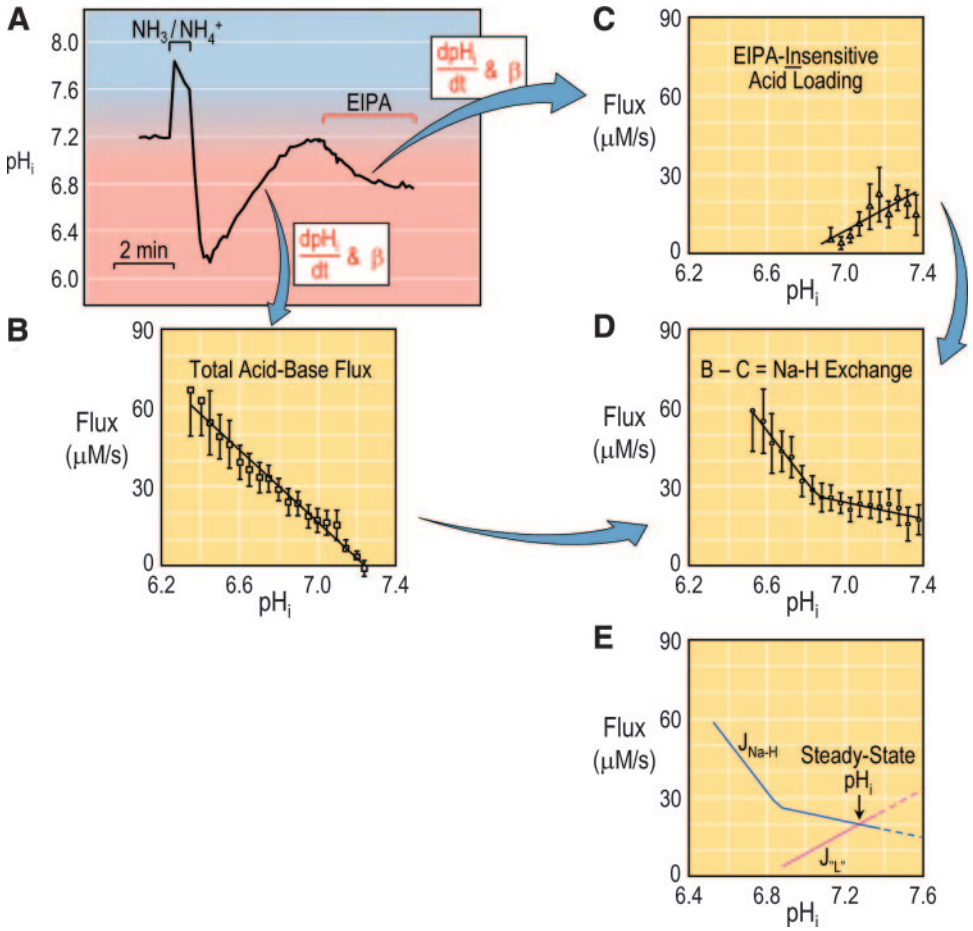

Fig. 15. Isolating the effects of Na-H exchange from those of other entities that may influence pH_i. *A*: representative experiment on a single renal mesangial cell (the same data as presented in Fig. 14*B*). *B*: summary of data for total acid-base flux. In several experiments similar to that shown in *A*, the investigators determined the rate of pH_i increase (i.e., dpHi/d*t*) at several discrete pH_i values during the pH_i recovery from the NH_3/NH_4^+ pulse. At each pH_i value, they multiplied the dpH_i/dt by the total intracellular buffering power (β) to obtain the total acid-base flux in micromoles of acid equivalents per second per liter of cytosol. At each pH_i value, these data were averaged, to produce the plot shown here. *C*: summary of data for EIPA-insensitive acid loading. In several experiments similar to that shown in *A*, the investigators determined the rate of pH_i decline during the exposure to EIPA at several discrete pH_i values. At each pH_i value, they multiplied the negative dpH_i/dt by the total intracellular buffering power (β) to obtain the total acid-base flux. At each pH_i value, these data were averaged, to produce the plot shown here. *D*: computed pH_i dependence of Na-H exchange, defined as the EIPA-sensitive acid-base flux. The data in this plot was obtained by subtracting the data in *C* from that in *B*. *E*: pH_i dependence of Na-H exchange and EIPA-insensitive acid loading. This panel is analogous to Fig. 1*B* in the temperature-regulation model. The $J_{Na\text{-}H}$-vs.-pH_i plot replaces the plot of the heat output of the furnace in Fig. 1*B*. Similarly, the $J_{"L"}$-vs-pH_i plot replaces the plot of the cold output of the air conditioner in Fig. 1*B*. Note that $J_{"L"}$ is not the true chronic acid-loading rate, but the *net* chronic acid-loading rate after the subtraction of Na-H exchange. The solid portion of the $J_{"L"}$ plot is the line of best fit in *C*; the dashed line is an extrapolation of the $J_{"L"}$ plot in *C*. The solid portion of the $J_{Na\text{-}H}$ plot consists of the two line segments of best fit in *D*; the dashed line is an extrapolation of the $J_{Na\text{-}H}$ plot in *D*. Data in *B*–*D* modified from Ref. 13.

Fig. 1*B*–the transporter is still active at values above the normal resting pH_i.

The fundamental law of pH_i regulation. Just as we introduced the fundamental law of temperature regulation (*Eq. 6*), we can introduce the fundamental law of pH_i regulation

$$\frac{\Delta pH_i}{\Delta t} = \frac{J_E - J_L}{\beta} \qquad (21)$$

which, in differential format, becomes

$$\frac{dpH_i}{dt} = \frac{J_E - J_L}{\beta} \qquad (22)$$

In other words, at any instant in time, the rate of pH_i change is proportional to the difference between the acid-extrusion and acid-loading rates, and inversely proportional to the total intracellular buffering power. If J_E equals J_L, pH_i is stable.

Changes in steady-state pH_i (temperature). In our discussion of temperature regulation, we noted that the only way to change steady-state temperature is to alter the fundamental kinetics of J_{heat} and/or J_{cold}. The analogous rule is true as well for pH_i: the only way to alter steady-state pH_i is to alter the fundamental kinetics of J_E and J_L.

Effect of the ras oncogene. A particularly striking example of a shift in steady-state pH_i is seen when comparing wild-type 3T3 fibroblasts with counterparts transformed with the c-H-*ras* oncogene (23). Whether the cells were incubated in a CO_2/HCO_3^--free or a CO_2/HCO_3^--containing medium, the *ras*-transformed cells had a steady-state pH_i that was about a half pH unit more alkaline than the untransformed parental cells. Figure 16 summarizes an analysis in which Kaplan and Boron used an ammonium prepulse to acid load the two populations of cells that they incubated in a CO_2/HCO_3^- medium. Because the cells were in a HCO_3^--containing medium, two acid-extrusion mechanisms were functioning: a Na-H exchanger and a Na^+-coupled HCO_3^- transporter. This situation is analogous to having a house with two furnaces.

The experimental approach was similar to the one we discussed in Fig. 15, except that the investigators determined the components of the subsequent pH_i recovery that were blocked either by EIPA (which blocks Na-H exchange) or by 5,5′-diisothiocyanatostilbene-2,2′-disulfonate (which blocks several HCO_3^- transporters). Transformation with oncogenic *ras* alkaline-shifted the pH_i profile of Na-H exchange by ~0.7 pH units. This change is analogous to shifting the temperature profile of a furnace so that it continues to produce heat at high rates even at very high temperatures. The transformation with *ras* also caused a marked alkaline shift in the pH_i profile of HCO_3^- uptake. Thus, by modulating the kinetics of both Na-H exchange and Na^+-coupled HCO_3^- uptake, oncogenic *ras* caused a striking increase in the steady-state pH_i. The benefit of these changes to a cancerous cell is that it might better be able to withstand the acidic environment of a solid tumor (19, 40). Another possibility, which is not mutually exclusive, is that an upward shift in pH_i could serve a signaling function for the cell.

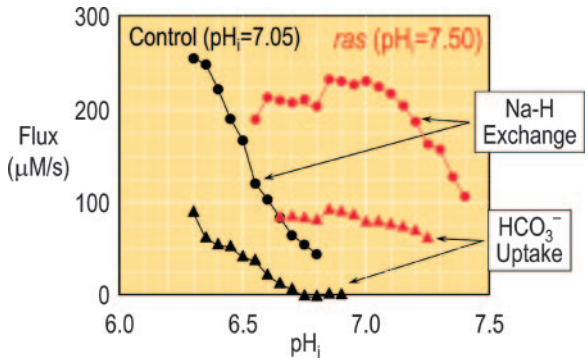

Fig. 16. The pH_i dependence of acid-extrusion rates in NIH-3T3 fibroblasts. The solid symbols represent the parental 3T3 cells, whereas the red symbols represent cells transformed with the c-H-*ras* oncogene. The flux due to Na-H exchange was taken as the flux sensitive to 50 μM EIPA, whereas the flux due to HCO_3^- uptake was taken as the flux sensitive to 50 μM DIDS. Data modified from Ref. 23.

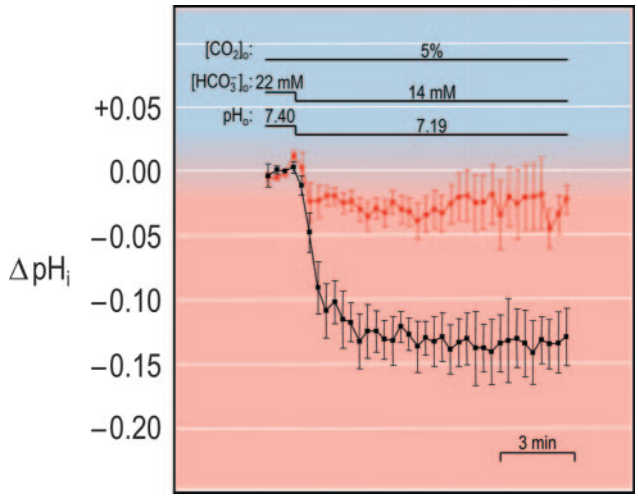

Fig. 17. Effect of metabolic acidosis on cultured hippocampal neurons from rat. The black points represent data from 4 neurons that had a large pH_i response to metabolic acidosis, whereas the red points represent data from 5–10 neurons that had a small pH_i response to metabolic acidosis. Data modified from Ref. 12.

Effect of metabolic acidosis. It has long been known that when cells are subjected to respiratory acidosis (a fall in pH_o caused by an increase in P_{CO_2}) or metabolic acidosis (a fall in pH_o caused by a decrease in $[HCO_3^-]_o$ at a fixed P_{CO_2}), pH_i falls as well (36). Conversely, it has long been known that when cells are subjected to respiratory alkalosis (a rise in pH_o caused by a decrease in P_{CO_2}) or metabolic alkalosis (a rise in pH_o caused by an increase in $[HCO_3^-]_o$ at a fixed P_{CO_2}), pH_i rises as well. By analogy to our temperature model, we may regard the ratio $\Delta pH_i/\Delta pH_o$ as an index of pH_i stability:

$$pH_i \text{ stability} = \frac{\Delta pH_i}{\Delta pH_o} \qquad (23)$$

$\Delta pH_i/\Delta pH_o$ is generally ~30%. However, in many pH-sensitive cells, such as the glomus cells of the peripheral chemoreceptor (14), or certain neurons in pH-sensitive brain regions (31, 32), $\Delta pH_i/\Delta pH_o$ may be twice as large.

Figure 17 summarizes data from experiments conducted by Bouyer et al. (12) on cultured hippocampal neurons, the firing rate of which exhibits little sensitivity to changes in pH_o (47). Quite surprisingly, subjecting the neurons to metabolic acidosis elicited one of two very different responses. A minority of

the neurons (~30%, black symbols) exhibited the expected response, a relatively large pH_i decrease that corresponds to a $\Delta pH_i/\Delta pH_o$ of ~0.60. In these cells, the large fall in steady-state pH_i presumably occurred because the decreases in pH_o and $[HCO_3^-]_o$ caused a decrease in acid extrusion and/or an increase in acid loading. In other words, a fundamental change in the kinetics of J_E and/or J_L led to a shift in steady-state pH_i.

The majority of the hippocampal neurons (~70%, red symbols) exhibited relatively little pH_i decline, corresponding to a $\Delta pH_i/\Delta pH_o$ of only ~0.01. The ability of the neurons to resist the metabolic acidosis presumably reflects some adaptation of J_E and/or J_L, an issue that we will discuss in the next Section.

CO_2 and HCO_3^- (environmental) sensors. A wide variety of signal-transduction systems impinge on the pH_i-regulating machinery of various cell types. The *ras* oncogene (see Fig. 16) is just one example. These signal-transduction systems allow acid-base transporters to respond to various hormones, growth factors and even to signals generated within the cell.

Ongoing work in our laboratory suggests that at least certain cells may have sensors that allow them to respond to changes in extracellular $[CO_2]$ or extracellular $[HCO_3^-]$ akin to the snow and sun sensors that we discussed in our temperature-regulation model. The key tool for beginning to elucidate these sensors is a technique that our laboratory developed for generating *out-of-equilibrium* (OOE) CO_2/HCO_3^- solutions (48). The OOE approach exploits the slow equilibrium $CO_2 + H_2O \rightleftarrows H_2CO_3$. As shown in Fig. 18, the approach is to mix two dissimilar solutions, and deliver the mixture to the cells so rapidly that the CO_2, HCO_3^-, and H^+ in the mixture does not have time to come into equilibrium.

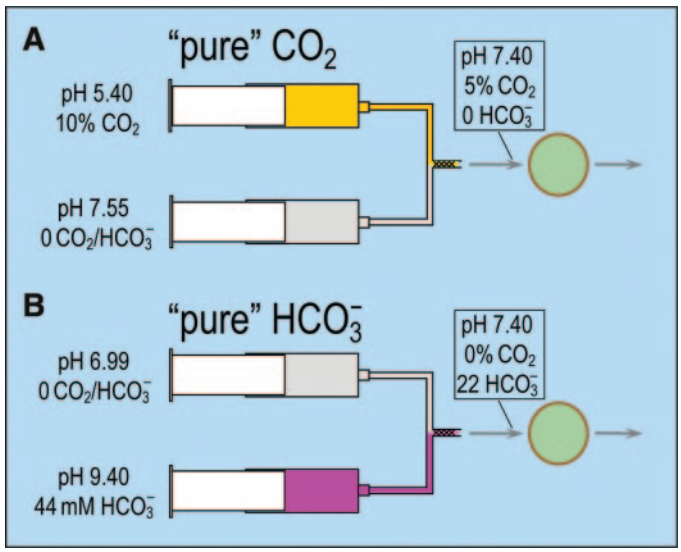

Fig. 18. Generating out-of-equilibrium CO_2/HCO_3^- solutions. *A*: generating a "pure" CO_2 solution. *B*: generating a "pure" HCO_3^- solution. In both *A* and *B*, a dual syringe pump causes the contents of two syringes to mix at the "T". Downstream from the "T", nylon mesh inside the tubing insures thorough mixing before the solutions reach the cells. After the solutions pass the cells, they are sucked away. Because the solutions are flowing very rapidly (7.0 ml/min), the solution newly created at the "T" does not have time to come into equilibrium before reaching the cells (time from mixing to cells <200 ms). Thus, one is able to control $[CO_2]$, $[HCO_3^-]$, and pH independently. The values in the two boxes indicate the idealized values of pH, $[CO_2]$, and $[HCO_3^-]$ at the time each of the two out-of-equilibrium solutions reaches the cells. We estimate that, by the time the "pure" CO_2 solution reaches the cells, the reaction $CO_2 + H_2O \rightarrow HCO_3^- + H^+$ has had time to increase $[HCO_3^-]$ to ~1% of the standard value of 22 mM (which, with 5% CO_2, would yield a pH of 7.40). Similarly, we estimate that, by the time the "pure" HCO_3^- solution reaches the cells, the reaction $HCO_3^- + H^+ \rightarrow CO_2 + H_2O$ has had time to increase $[CO_2]$ to ~0.1% of the standard value of 5% (which, with 22 mM HCO_3^-, would yield a pH of 7.40). Modified from Ref. 49.

Experiments on renal proximal tubules. One preparation that has yielded quite interesting results with OOE solutions has been the isolated, perfused renal proximal tubule. One can perfuse the lumen of a single, hand-dissected tubule with a solution containing equilibrated CO_2 and HCO_3^-, as well as ^{3}H-methoxyinulin as a volume marker. After the solution has been collected after it has passed along the lumen of the tubule, one can assay for HCO_3^- and ^{3}H, and then compute the rate of volume reabsorption (J_V, the amount of water per minute that disappears from the tubule lumen) and the rate of HCO_3^- reabsorption ($JHCO_3$, the amount of HCO_3^- per minute that disappears from the tubule lumen) (49). We used the OOE approach to change—one at a time—the pH, $[HCO_3^-]$, and $[CO_2]$ on the basolateral (i.e., blood-side) aspect of the tubule. We found that isolated increases in basolateral (BL) $[HCO_3^-]$ cause $JHCO_3$ to fall (53), which would make teleological sense (i.e., high $[HCO_3^-]$ in the blood ought to signal the tubule to reabsorb less HCO_3^- from lumen to blood). We also found that isolated increases in $[CO_2]_{BL}$ cause $JHCO_3$ to rise, which also would make teleological sense (i.e., high $[CO_2]$ in the blood ought to signal the tubule to reabsorb more HCO_3^- and thereby help normalize blood pH).

In principle, this stimulation of HCO_3^- reabsorption by basolateral CO_2 could be a side effect of the fall in pH_i that occurs as one raises $[CO_2]_{BL}$. However, we were quite surprised to find that isolated changes in pH_{BL} have no effect on $JHCO_3$, even though these isolated changes in pH_{BL} caused marked changes in pH_i. Thus, it appears that, at least as far as $JHCO_3$ is concerned, the proximal-tubule cell is impervious to acute changes in pH, whether they be changes in basolateral pH or cytosolic pH. The sensitivity to changes in $[CO_2]_{BL}$ must therefore reflect the ability of the cell to sense CO_2 per se. Inasmuch as other lines of evidence suggest that the tubule is insensitive to CO_2 in the lumen (15, 16), the most likely explanation is that proximal-tubule cells have some sort of mechanism for sensing CO_2 per se at or near the basolateral membrane.

In response to an increase in $[CO_2]_{BL}$, the tubule cell presumably increases the transport rate of one or more of the transporters involved in the reabsorption of HCO_3^-: a Na-H exchanger and a vacuolar-type H^+ pump at the apical membrane (these extrude acid into the lumen, thereby titrating HCO_3^- to CO_2 and H_2O), and an electrogenic Na/HCO_3 cotransporter at the basolateral membrane (the pathway for HCO_3^- to enter the blood). Further work indicates that the ability of the tubule to respond to changes in $[CO_2]_{BL}$ is blocked by nanomolar levels of certain agents that block a restricted group of tyrosine kinases (50, 51), and is also blocked by procedures that interfere with the ability of luminal angiotensin II to activate its receptor (52). Of course, it would be interesting to know the identity of the CO_2-sensor molecule, as well as to know the precise signal-transduction cascade used to stimulate the acid-base transporters.

Experiments on cultured hippocampal neurons. As noted earlier, the data represented by the red symbols in Fig. 17 indicate that most hippocampal neurons have the ability to resist the expected effects of *metabolic* acidosis on pH_i. How-

ever, all hippocampal neurons exhibit a large pH_i decrease in response to *respiratory* acidosis, and all neurons exhibit a large pH_i increase in response to both metabolic and respiratory alkalosis. A line of reasoning too tedious for the present forum suggests the neurons that have unusually small responses to metabolic acidosis do so because they are able to detect the decrease in $[HCO_3^-]_o$ per se. Indeed, preliminary work shows that neurons resistant to metabolic acidosis have an unusual response to an OOE solution that has a normal $[CO_2]_o$, a normal pH_o but a low $[HCO_3^-]_o$: in these neurons, an isolated decrease in $[HCO_3^-]_o$ causes pH_i to rise by ~0.15.

The above result is as unexpected as observing that lowering $[Ca^{2+}]_o$ causes $[Ca^{2+}]_i$ to rise, and suggests that these neurons have a mechanism for directly sensing changes in $[HCO_3^-]_o$ per se. These neurons come from a part of the brain well known for exhibiting long-term potentiation, a primitive form of memory. The unusual neurons evidently do not care about pH_i changes triggered by changes in $[CO_2]_o$. Nor do they care about increases in pH_i caused by increases in $[HCO_3^-]_o$. However, they seem to be carefully defending pH_i against the decrease that would otherwise result from lowering $[HCO_3^-]_o$. It would be very interesting to know the identity of the HCO_3^- sensor, and the signal transduction pathways it uses. Nevertheless, based on the logic that we developed in our temperature-regulation model, we can conclude that these unusual neurons must respond to decreases in $[HCO_3^-]_o$ by stimulating acid extrusion and/or inhibiting acid loading.

In conclusion, as the reader may glean from the second half of this article, the field of pH_i regulation is quite complex, and is becoming ever more complex as we better understand the molecular mechanisms by which the acid-base transport proteins function, and learn more about how protein-protein interactions and a wide range of signal-transduction systems influence these transporters. It is indeed sometimes a challenge to integrate the effects of molecular changes in such a way that one can accurately predict the effects on pH_i regulation. At times such as these, it is useful to remember that pH_i regulation is not as complicated as it is sometimes cracked up to be. Just keep track of those furnaces and air conditioners, and you will do just fine.

ACKNOWLEDGMENTS

I thank Duncan Wong for helping with the figures and for other computer-related assistance. I am also grateful to Patrice Bouyer and Michelle Messier for comments on an earlier version of the manuscript.

GRANTS

This work was supported by National Institutes of Health Grants HD-32573, NS-18400, DK-17433, and DK-30344.

REFERENCES

1. **Aalkjær C and Hughes A.** Chloride and bicarbonate transport in rat resistance arteries. *J Physiol* 436: 57–73, 1991.
2. **Apkon M and Boron WF.** Extracellular and intracellular alkalinization and the constriction of rat cerebral arterioles. *J Physiol* 484: 743–753, 1995.
3. **Apkon M, Weed RA, and Boron WF.** Motor responses of cultured rat cerebral vascular smooth muscle cells to intra- and extracellular pH changes. *Am J Physiol Heart Circ Physiol* 273: H434–H445, 1997.
4. **Boron WF.** Intracellular pH transients in giant barnacle muscle fibers. *Am J Physiol Cell Physiol* 233: C61–C73, 1977.
5. **Boron WF.** Acid-base physiology. In: *Medical Physiology. A Cellular and Molecular Approach*, edited by Boron WF and Boulpaep EL. Philadelphia, PA: Saunders, p. 633–653, 2003.
6. **Boron WF and Boulpaep EL.** Intracellular pH regulation in the renal proximal tubule of the salamander: basolateral HCO_3^- transport. *J Gen Physiol* 81: 53–94, 1983.
7. **Boron WF and De Weer P.** Active proton transport stimulated by CO_2/HCO_3^- blocked by cyanide. *Nature* 259: 240–241, 1976.
8. **Boron WF and De Weer P.** Intracellular pH transients in squid giant axons caused by CO_2, NH_3 and metabolic inhibitors. *J Gen Physiol* 67: 91–112, 1976.
9. **Boron WF, McCormick WC, and Roos A.** pH regulation in barnacle muscle fibers: dependence on intracellular and extracellular pH. *Am J Physiol Cell Physiol* 237: C185–C193, 1979.
10. **Boron WF, McCormick WC, and Roos A.** pH regulation in barnacle muscle fibers: dependence on extracellular sodium and bicarbonate. *Am J Physiol Cell Physiol* 240: C80–C89, 1981.
11. **Boron WF and Russell JM.** Stoichiometry and ion dependencies of the intracellular-pH-regulating mechanism in squid giant axons. *J Gen Physiol* 81: 373–399, 1983.
12. **Bouyer P, Bradley SR, Zhao J, Wang W, Richerson GB, and Boron WF.** Effect of extracellular acid-base disturbances on the intracellular pH of neurones cultured from rat medullary raphe or hippocampus. *J Physiol* 559: 85–101, 2004.
13. **Boyarsky G, Ganz MB, Cragoe EJ Jr, and Boron WF.** Intracellular pH dependence of Na-H exchange and acid loading in quiescent and arginine vasopressin-activated mesangial cells. *Proc Natl Acad Sci USA* 87: 5921–5924, 1990.
14. **Buckler KJ, Vaughan-Jones RD, Peers C, Lagadic-Gossmann D, and Nye PCG.** Effects of extracellular pH, P_{CO_2} and HCO_3^- on intracellular pH in isolated type-1 cells of the neonatal rat carotid body. *J Physiol* 444: 703–721, 1991.
15. **Chen LK and Boron WF.** Acid extrusion in S3 segment of rabbit proximal tubule. I. Effect of bilateral CO_2/HCO_3^-. *Am J Physiol Renal Fluid Electrolyte Physiol* 268: F179–F192, 1995.
16. **Chen LK and Boron WF.** Acid extrusion in S3 segment of rabbit proximal tubule: II. Effect of basolateral CO_2/HCO_3^-. *Am J Physiol Renal Fluid Electrolyte Physiol* 268: F193–F203, 1995.
17. **Choi I, Aalkjær C, Boulpaep EL, and Boron WF.** An electroneutral sodium/bicarbonate cotransporter NBCn1 and associated sodium channel. *Nature* 405: 571–575, 2000.
18. **Deitmer JW and Schlue WR.** An inwardly directed electrogenic sodium-bicarbonate cotransport in leech glial cells. *J Physiol* 411: 179–194, 1989.
19. **Gillies RJ, Martínez-Zaguilán R, Peterson EP, and Perona R.** Role of intracellular pH in mammalian cell proliferation. *Cell Physiol Biochem* 2: 159–179, 1992.
20. **Grichtchenko II, Choi I, Zhong X, Bray-Ward P, Russell JM, and Boron WF.** Cloning, characterization, and chromosomal mapping of a human electroneutral Na^+-driven Cl-HCO_3 exchanger. *J Biol Chem* 276: 8358–8363, 2001.
21. **Gross E, Hawkins K, Abuladze N, Pushkin A, Cotton CU, Hopfer U, and Kurtz I.** The stoichiometry of the electrogenic sodium bicarbonate cotransporter NBC1 is cell-type dependent. *J Physiol* 531: 597–603, 2001.
22. **Han J, Kang D, and Kim D.** Functional properties of four splice variants of a human pancreatic tandem-pore K^+ channel, TALK-1. *Am J Physiol Cell Physiol* 285: C529–C538, 2003.
23. **Kaplan D and Boron WF.** Long-term expression of c-H-ras stimulates Na-H and Na^+-dependent Cl-HCO_3 exchange in NIH-3T3 fibroblasts. *J Biol Chem* 269: 4116–4124, 1994.
24. **Kopito RR and Lodish HF.** Primary structure and transmembrane orientation of the murine anion exchange protein. *Nature* 316: 234–238, 1985.
25. **Krishtal OA and Pidoplichko VI.** A receptor for protons in the membrane of sensory neurons may participate in nociception. *Neuroscience* 6: 2599–2601, 1981.
26. **Lesage F.** Pharmacology of neuronal background potassium channels. *Neuropharmacology* 44: 1–7, 2003.
27. **Murer H, Hopfer U, and Kinne R.** Sodium/proton antiport in brush-border-membrane vesicles isolated from rat small intestine and kidney. *Biochem J* 154: 597–604, 1976.
28. **Orlowski J and Grinstein S.** Diversity of the mammalian sodium/proton exchanger SLC9 gene family. *Pflügers Arch* 447: 549–565, 2004.
29. **Pushkin A, Abuladze N, Lee I, Newman D, Hwang J, and Kurtz I.** Cloning, tissue distribution, genomic organization, and functional characterization of NBC3, a new member of the sodium bicarbonate cotransporter family. *J Biol Chem* 274: 16569–16575, 1999.

30. **Rajan S, Wischmeyer E, Xin LG, Preisig-Müller R, Daut J, Karschin A, and Derst C.** TASK-3, a novel tandem pore domain acid-sensitive K^+ channel. An extracellular histidine as pH sensor. *J Biol Chem* 275: 16650–16657, 2000.
31. **Ritucci NA, Chambers-Kersh L, Dean JB, and Putnam RW.** Intracellular pH regulation in neurons from chemosensitive and nonchemosensitive areas of the medulla. *Am J Physiol Regul Integr Comp Physiol* 275: R1152–R1163, 1998.
32. **Ritucci NA, Dean JB, and Putnam RW.** Intracellular pH response to hypercapnia in neurons from chemosensitive areas of the medulla. *Am J Physiol Regul Integr Comp Physiol* 273: R433–R441, 1997.
33. **Romero MF, Fulton CM, and Boron WF.** The SLC4 family of HCO_3^- transporters. *Pflügers Arch* 447: 495–509, 2004.
34. **Romero MF, Hediger MA, Boulpaep EL, and Boron WF.** Expression cloning and characterization of a renal electrogenic Na^+/HCO_3^- cotransporter. *Nature* 387: 409–413, 1997.
35. **Romero MF, Henry D, Nelson S, Harte PJ, Dillon AK, and Sciortino CM.** Cloning and characterization of a Na^+-driven anion exchanger (NDAE1). A new bicarbonate transporter. *J Biol Chem* 275: 24552–24559, 2000.
36. **Roos A and Boron WF.** Intracellular pH. *Physiol Rev* 61: 296–434, 1981.
37. **Russell JM and Boron WF.** Role of chloride transport in regulation of intracellular pH. *Nature* 264: 73–74, 1976.
38. **Russell JM, Boron WF, and Brodwick MS.** Intracellular pH and Na fluxes in barnacle muscle with evidence for reversal of the ionic mechanism of intracellular pH regulation. *J Gen Physiol* 82: 47–78, 1983.
39. **Sardet C, Franchi A, and Pouysségur J.** Molecular cloning, primary structure, and expression of the human growth factor-activatable Na^+/H^+ antiporter. *Cell* 56: 271–280, 1989.
40. **Stubbs M, McSheehy PM, Griffiths JR, and Bashford CL.** Causes and consequences of tumour acidity and implications for treatment. *Mol Med Today* 6: 15–19, 2000.
41. **Thomas RC.** Ionic mechanism of the H^+ pump in a snail neurone. *Nature* 262: 54–55, 1976.
42. **Thomas RC.** The effect of carbon dioxide on the intracellular pH and buffering power of snail neurones. *J Physiol* 255: 715–735, 1976.
43. **Thomas RC.** The role of bicarbonate, chloride and sodium ions in the regulation of intracellular pH in snail neurones. *J Physiol* 273: 317–338, 1977.
44. **Vaughan-Jones RD.** Regulation of chloride in quiescent sheep-heart Purkinje fibres studied using intracellular chloride and pH-sensitive microelectrodes. *J Physiol* 295: 111–137, 1979.
45. **Vaughan-Jones RD.** Chloride-bicarbonate exchange in the sheep cardiac Purkinje fibre. In: *Intracellular pH: Its Measurement, Regulation and Utilization in Cellular Functions*, edited by Nuccitelli R. New York: Liss, 1982, p. 239–252.
46. **Waldmann R, Champigny G, Bassilana F, Heurteaux C, and Lazdunski M.** A proton-gated cation channel involved in acid-sensing. *Nature* 386: 173–177, 1997.
47. **Wang W and Richerson GB.** Chemosensitivity of non-respiratory rat CNS neurons in tissue culture. *Brain Res* 860: 119–129, 2000.
48. **Zhao J, Hogan EM, Bevensee MO, and Boron WF.** Out-of-equilibrium CO_2/HCO_3^- solutions and their use in characterizing a new K/HCO_3 cotransporter. *Nature* 374: 636–639, 1995.
49. **Zhao J, Zhou Y, and Boron WF.** Effect of isolated removal of either basolateral HCO_3^- or basolateral CO_2 on HCO_3^- reabsorption by rabbit S2 proximal tubule. *Am J Physiol Renal Physiol* 285: F359–F369, 2003.
50. **Zhou Y, Bouyer P, and Boron WF.** CO_2-evoked increased in HCO_3 reabsorption in the rabbit S_2 proximal tubule: Blockade by genistein (Abstract). *FASEB J* 17: A1221, 2003.
51. **Zhou Y, Bouyer P, and Boron WF.** Role of a receptor tyrosine kinase in the CO_2-induced stimulation of HCO_3 reabsorption by rabbit S2 proximal tubules (Abstract). *FASEB J* 18: A1016, 2004.
52. **Zhou Y, Bouyer P, and Boron WF.** Role of endogenously secreted angiotensin II in the CO_2-induced stimulation of HCO_3 reabsorption by rabbit S2 proximal tubules (Abstract). *FASEB J* 18: A1016, 2004.
53. **Zhou Y, Zhao J, Bouyer P, and Boron WF.** Regulation of bicarbonate reabsorption by S2 proximal tubule: evidence for a CO_2-sensor (Abstract). *FASEB J* 15: A142, 2001.